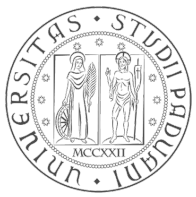

Università degli Studi di Padova

Dipartimento di Ingegneria dell'Informazione

Corso di Laurea Magistrale in
Ingegneria delle Telecomunicazioni

Wireless Power Transfer for Next Generation Mobile Networks:
Heuristic Policies and their Performance Analysis

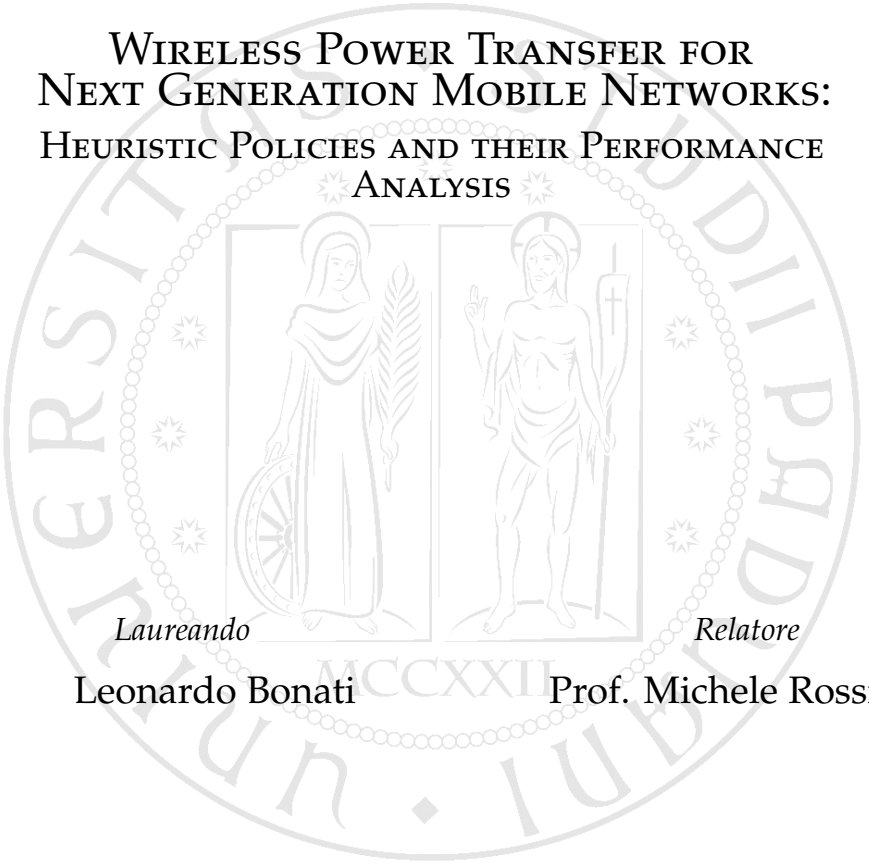

Laureando

Leonardo Bonati

Relatore

Prof. Michele Rossi

10 Ottobre 2016

Anno Accademico 2015/2016

ABSTRACT

In this work we study Wireless Power Transfer for Next Generation Mobile Networks. This technique permits to charge mobile devices without the need to connect them to an external power source, such as the electrical grid. We consider the case in which many users travel along the network, where a certain number of base stations has been deployed. The users' mobile devices, whose battery naturally keeps discharging as time goes on, upon reaching a certain battery energy threshold, issue a charging request to the base stations they can reach out. These, in addition to relying the devices' information, can also wirelessly transfer power to them. When a base station receives a charging request, it has to decide whether to transfer energy to the requiring device, thus charging it, or not. In order to allow the base stations to make this decision, we design some heuristic policies and analyse their performance and the way the network reacts to them. We also mention some interesting applications and developments of these techniques.

CONTENTS

1 INTRODUCTION

Nowadays Internet counts more than 3 billions active users in the world, sending more than 2 millions emails and watching more than 130 thousands YouTube videos per second [15]. The largest part of the overall Internet traffic is generated by mobile devices, that have almost completely replaced fixed computers in the average users' lives.

These devices, either being smartphones, tablets or wearable ones, are battery-powered and tend to discharge quite rapidly. This fact usually forces their owners to connect them to an external electrical source during the day, maybe just for a short period of time, to gain that extra energy that permits the devices to safely reach the end of the day, when they will be plugged in and be fully charged. However, connecting a device to an energy source in the middle of the day is a not-always-possible operation, due to the fact that the mobile user has to move from one place to another, or simply forgot the charger at home.

Wireless Power Transfer (WPT) is a cutting-edge technique that permits to charge a mobile device without the need to connect it to any external power supply and, in some cases, without the user even being aware of it. This relies on external tools, such as power mats or base stations, that are able to communicate with the User Equipment (UE) and charge it by sending power wirelessly, if necessary.

In this work, we study this highly innovative technique applied to next generation mobile networks, considering a scenario in which base stations are placed around the network and mobile devices ask them to be wirelessly charged when they present low battery levels. More specifically, we design heuristic policies from scratch, that allow the base stations to decide whether, when and how to charge the energy-requiring nodes, also analysing their performance and possible implementation in real-world applications.

The remaining part of this dissertation is organised as follows. In Chapter 2 we analyse the most common techniques to charge devices through WPT, in Section 2.1, explore the state-of-the-art applications of this method, in Section 2.2, and define our intended scenario, in Section 2.3. Chapter 3 thoroughly

describes the mathematical model we built to study this problem, particularly focusing on the users' mobility models, in Section 3.2, and on the designed charging policies, in Section 3.4. In Chapter 4 we present and discuss some relevant results selected among the ones obtained from the run experiments. In particular, we considered a normal mobility scenario, in Section 4.1 and a slow mobility one, in Section 4.2. Finally, Chapter 5 concludes our work, reporting some final remarks and possible future developments and applications of these techniques.

2

STATE OF THE ART

Wireless Power Transfer (WPT) is a technique that involves a transmitter, that sends power through the wireless channel, and at least one receiver, that harvests it to replenish its battery. We discuss the commonly used techniques for wireless charging in Section 2.1, while we explore literature solutions involving WPT in Section 2.2 and, finally, in Section 2.3 we define the considered scenario.

2.1 WIRELESS CHARGING TECHNIQUES

The literature reports three main techniques for wireless charging [24]: *Magnetic Inductive Coupling* and *Magnetic Resonance Coupling* for the near field, and *Microwave Radiation* for the far field.

2.1.1 *Magnetic Inductive Coupling*

Magnetic inductive coupling is based on magnetic field induction, which exploits two aligned coils, one at the transmitter, i.e., the charger, and the other one at the receiver, i.e., the device to be charged, to transfer electrical energy. At the transmitter, a primary coil of conductive material is connected to an Alternating Current (AC) power source and generates an oscillating magnetic field. At the receiver, a secondary coil, close to the primary one, experiences an oscillating magnetic flux. Variations in this flux traversing the secondary coil induce an electric current, that can be used to charge a device's battery. The aforementioned scheme is shown in Figure 1.

V_S, L_S, R_L and L_L are the voltage and the inductance on the transmitter side and the resistance and the inductance on the receiver side, respectively.

The induced current on the receiving circuit, I_L, can be computed as [16]:

$$I_L(R_L + j\omega L_L + z_L) = j\omega M I_S, \tag{1}$$

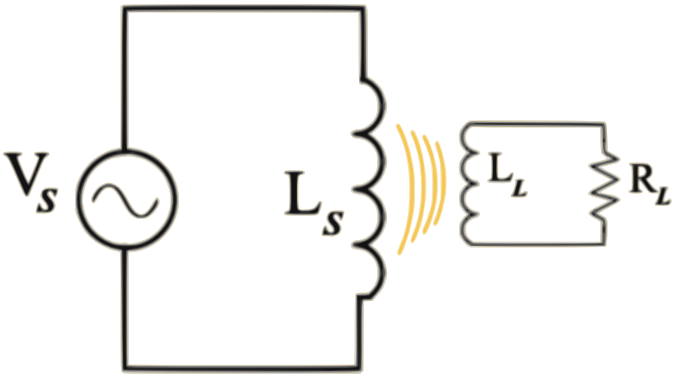

Figure 1: Inductive charging circuit, from [16].

from which:

$$I_L = \frac{j\omega M I_S}{R_L + j\omega L_L + z_L}, \tag{2}$$

where I_S is the current on the transmitting circuit, while z_L and M respectively are the complex impedance on the receiving circuit and the mutual inductance coefficient, i.e., how much the two circuits are magnetically coupled. Finally, ω is the angular frequency of the system and j is the imaginary unit. Due to magnetic coupling, the receiver affects the transmitter as well in the following way [16]:

$$V_S = I_S(j\omega L_S + z_S) - j\omega M I_L, \tag{3}$$

where z_S is the complex inductance on the transmitter side.

The energy efficiency of this scheme depends on the coupling tightness between the two coils and on their quality factor. The former is determined by the alignment and the distance between the two coils, their diameter ratio and shape, while the latter by the building materials of the coils and their operating frequency.

Magnetic inductive coupling is safe to use, offers ease of implementation and a high efficiency at close distance, i.e., shorter than the coil's diameter, usually $7mm$ [32]. Recently developed techniques, such as MagMIMO [16], though, claim to be able to charge a device up to $40cm$ away from the charger.

However, one of the main disadvantages of current solutions for magnetic inductive coupling is that the two coils need to be aligned, i.e., the device to be charged has to be put on a precise spot of the charging area, although some transmitters use multiple-coils systems, thus eliminating this need [32].

2.1.2 *Magnetic Resonance Coupling*

Magnetic resonance coupling is based on evanescent-wave coupling, i.e., the coupling between two waves due to physical overlap, which, through varying or oscillating magnetic fields, generate and transfer electrical energy between two resonant coils. Compared with the scheme shown in Figure 1, capacitances, that are induced to resonate at the same frequency, are included in both the transmitter and receiver circuits. At the transmitter side, once the applied voltage triggers the oscillation, the circuit keeps resonating back and forth without consuming any additional energy [16]. The described scheme is shown in Figure 2.

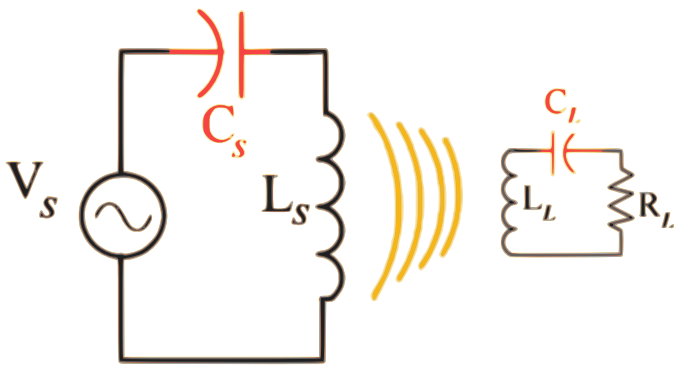

Figure 2: Resonant charging circuit, from [16].

The same notation of Section 2.1.1 is adopted. C_S is the capacitance on the transmitting circuit, while C_L is the one on the receiving circuit.

The induced current at the receiving circuit, I_L, can be computed as follows [16]:

$$I_L(R_L + j\omega L_L + \frac{1}{j\omega C_L} + z_L) = j\omega M I_S, \tag{4}$$

from which:

$$I_L = \frac{j\omega M I_S}{R_L + j\omega L_L + \frac{1}{j\omega C_L} + z_L} \tag{5}$$

Analogously to what described in Section 2.1.1, the transmitting circuit is affected as well in the following way [16]:

$$V_S = I_S(j\omega L_S + \frac{1}{j\omega C_S} + z_S) - j\omega M I_L, \tag{6}$$

where the same notation used in Section 2.1.1 is also adopted in Equations 4, 5 and 6. Due to the fact that the two circuits operate at the resonating frequency, the terms $j\omega L_L$ and $\frac{1}{j\omega C_L}$ in Equations 4 and 5 cancel each other and so do the terms $j\omega L_S$ and $\frac{1}{j\omega C_S}$ in Equation 6.

The two coils are strongly coupled, thus enabling this technique to obtain a high energy transfer efficiency, to be immune to the neighbour environment and not to require Line of Sight (LoS).

Magnetic resonance coupling permits to transfer energy at a greater distance than what possible using traditional magnetic inductive coupling, in fact, implemented solutions report to be able to charge a device whose distance from the charger is up to 45mm [32]. This technique also permits to charge multiple devices at once by properly tuning the coupling resonators of multiple receiving coils and, thus, avoiding interference between these [20].

2.1.3 *Microwave Radiation*

Microwave radiation [24] exploits Radio Frequency (RF) waves, which frequency f ranges between 300MHz and 300GHz, that propagate at the speed of light, to carry radiant energy.

In this technique, the transmitter first performs an AC/DC conversion and then a DC/RF one through a *magnetron*, i.e., a vacuum tube that generates microwaves when stimulated by a current. These are propagated through the air and captured, at the receiver side, by a *rectenna*, that converts them into Direct Current (DC) electricity. Microwaves can radiate energy in all directions isotropically, making them ideal for broadcast applications, or toward a specific one through beamforming, for point-to-point transmission. This last approach, called *power beamforming*, can greatly improve the transmission efficiency.

Microwave radiation can reach longer distances than the methods described in Sections 2.1.1 and 2.1.2, and, by performing a low-power and long-distance transfer, is able to power a large number of devices using a low amount of energy [25]. It is also compatible with the existing communication systems [24] and can deliver both energy and information at the same time using an approach called Simultaneous Wireless Information and Power Transfer (SWIPT) [44]. To this purpose, the amplitude of phase of microwaves is used to modulate information, while their radiation and vibration are used to carry energy [39].

The amount of received power depends on the transmitted one, the used wavelength and the distance between transmitter and receiver. In free space it can be computed using the Friis equation [40]:

$$P_{RX} = P_{TX} \frac{G_{TX} G_{RX} \lambda^2}{(4\pi d)^2}, \tag{7}$$

where P_{TX} is the transmitted power, G_{TX} and G_{RX} respectively represent the transmit and receive antenna gains, λ is the wavelength and d is the distance between the two antennas. For microwaves we have $\lambda \in [0.001, 1]m$. In indoor scenarios, instead, we also have to account for the path loss [40], given by:

$$P_L(dB) = 20 \log_{10}\left(\frac{4\pi d_0}{\lambda}\right) + 10n \log_{10}\left(\frac{d}{d_0}\right), \tag{8}$$

where d_0 is a reference distance and n is a constant that depends on the propagation environment. We have $n = 2$ for free space, $0.8 \leqslant n \leqslant 1.8$ for an indoor LoS environment and $n \leqslant 8.6$ for a non-LoS one [40].

Examples of commercial products using this technique are the Powercaster transmitter and the Powerharvester receiver, respectively used to transfer and collect RF power [31]. Examples of wireless power harvested from different sources are shown in Table 1.

Source	P_{TX} [W]	f [MHz]	d [m]	P_{RX} [μW]
Isotropic RF transmitter	4	$902 - 928$	15	5.5
Isotropic RF transmitter	1.78	868	25	2.3
Isotropic RF transmitter	1.78	868	27	2
Powercaster transmitter	3	915	5	189
Powercaster transmitter	3	915	11	1
KING-TV tower	$960 \cdot 10^3$	$674 - 680$	$4.1 \cdot 10^3$	60

Table 1: Experimental data of RF power harvesting, from [26].

However, due to health concerns regarding the RF radiation, the Effective Isotropic Radiated Power (EIRP) is subjected to some region-dependent restrictions based on the used frequency band, shown in Table 2.

f [MHz]	EIRP [W]	Region
865.0 – 865.6	0.10	Europe
865.6 – 867.6	2.00	Europe
867.6 – 868.0	0.50	Europe
2446.0 – 2454.0	4.00	Europe
902.0 – 928.0	4.00	USA, Canada
2400.0 – 2483.5	4.00	USA, Canada
2400.0 – 2483.5	0.01	Japan, Korea

Table 2: Transmit power restrictions for RFID applications, from [40].

2.2 LITERATURE REVIEW

Due to the large diffusion of the Wireless Sensor Networks (WSNs), to which the Internet of Things (IoT) paradigm surely contributed, involving relatively small and usually battery powered devices, various applications of WPT and energy harvesting arise from the literature, some of which can also be adapted for next generation mobile networks.

In [42], the authors study an optimization problem involving a single transmitter that harvests wireless energy from the network and, then, uses it to send data packets to a receiver. Two different scenarios are studied. In the first one packets are assumed to have already arrived at the transmitter and to be ready to be sent before the transmission starts, while in the second one they may also arrive during the transmission with known arrival times and sizes. Optimal offline scheduling policies to minimise the packet delivery time are developed.

In [41], instead, Xie et al. consider a set of nodes in the network and a fixed service station that functions as a sink for the nodes-generated data. The service station periodically sends out a mobile Wireless Charging Vehicle (WCV), equipped with WPT technology, to charge the nodes. The possible paths the WCV can travel along to reach the nodes are studied and it is shown that the shortest Hamiltonian cycle is the optimal path.

The authors of [13] consider an energy replenishment problem in mission-critical sensor networks, in which robots performing critical operations, such as life search and rescue, travel along the network. When the battery of these robots goes below a certain threshold, they ask a Mobile Charger (MC), equipped

with wireless transfer technology, to be charged. The MC, after collecting a certain number of requests from the various robots, or after a certain interval time has passed without receiving further requests, schedules the optimal path to reach these robots. The whole process does not require the emergency robots to modify their travelling path, but the MC adapts to it by choosing a rendezvous point belonging to the robots' programmed path, where the charging process will begin. Then, the MC follows the energy-requiring robot along its path until it completes charging it.

In [18], the authors consider a tour planning problem in a scenario in which the simultaneous on-demand charge of multiple nodes is involved. Here a MC, after collecting a certain number of requests from the nodes belonging to the WSN, computes the best travel path to charge them all. This approach, differently from other solutions that focus on shortening the charging delays, groups incoming charging requests and optimizes the charging tour and the energy consumption of the MC by maximising the number of nodes that is simultaneously charged. In this way, also if the charging delay is slightly increased, the nodes' failures are significantly reduced by taking advantage of the simultaneous charge of multiple sensors.

An handover management problem between macro, femto and pico cells is, instead, studied in [12]. In this situation a mobile user moves throughout a Heterogeneous Network (HetNet) and various policies to decide which type of cell to use to serve its requests are designed. Multiple parameters are taken into account to evaluate the handover decision, such as the user's mobility profile and speed, the power profile of the various cells or their traffic load. A Markov-based framework to model the handover process and an optimal context-dependent criterion are proposed. Finally, a handover strategy to maximise the UE average capacity as a function of the context parameters is developed. From this paper, the importance of context awareness to improve the handover process and to increase the mobile UEs' performance in heterogeneous networks clearly emerges.

The authors of [23] consider a problem in which a single base station is located at the centre of the cell and many relay nodes at its edge. The UEs move around the cell and harvest energy from RF transmission of the base station and the relay nodes and then use it for their own uplink transmission. Two different scenarios involving relay-based wireless-powered uplink cellular networks based on the harvest-then-transmit paradigm are

considered. In the first one, all the users harvest energy from the transmission coming from the base station and from the relay nodes, while in the second one cell-edge nodes only harvest energy from relay-nodes transmission and the users close to the centre of the cell only harvest energy from the base station. Different frameworks for resource allocation are proposed and optimal time and power allocations are derived for each case. The uplink throughput of all the UEs is also maximised. From the reported results it appears that most of the available resources, such as time and energy, have to be employed in the wireless charging process and that the second scenario performs better than the first one when optimal resource allocation is employed.

In [21], the authors consider a problem in which various sensors are deployed throughout the network and the aim is to charge them using a WCV, that comes close to the sensors and transfers power wirelessly to them. Instead of trying to maximise the number of devices the MC charges in a single step of the algorithm, they cluster the set of sensors into multiple groups containing few nodes, then the WCV travels to the centre of each set and charges the sensors. In this way, the average distance between the MC and the sensor that it is currently charging is minimised, thus obtaining a higher transfer efficiency with respect to the case in which the number of stops is minimised. The proposed scheme improves the non-clustered algorithm performance in terms of total and average charging time and journey time, i.e., the time the WCV spends travelling from one stop location to the next one.

In [24], a wireless charger network is considered in which fixed multiple chargers communicate among one another and with a centralised server, exchanging information on their availability to charge new devices, location, charging status and cost of charge. The server, that collects all the data coming from the chargers, is then able to assign a mobile UE the charger that best meets its requirements. Using this scheme the charging delay and the cost for the users to identify the best charger is minimised.

In [20], Kurs et al. exploit strongly coupled electromagnetic resonators to transfer power from a transmitter to a receiver separated by a distance much larger than the size of the resonators. This technique can also be used to remotely power multiple devices with a single transmitting source. The power transfer efficiency is experimentally shown for cases involving

coupling objects of different sizes. The authors also highlight that a single source powering many small devices, distributed over a large volume, achieves a good overall efficiency, even in situations in which the transfer efficiencies of the single devices are quite low.

In [16], Multiple Input Multiple Output (MIMO) beamforming is used to power mobile devices without needing them to be placed on apposite charging pads or with a particular orientation. This approach transfers power by beamforming the non-radiated magnetic field and steering it towards the mobile device. Differently than what is possible using traditional inductive or resonating approaches, where the device to be charged has to be placed close to the charger, with this technique a UE can be charged while inside its owner's pocket or inside a bag. With MagMIMO, in fact, the resonating magnetic field is focused on the receiving device to maximise the power transfer efficiency. Also, this technique does not require to modify the smartphones' hardware, but can be used with today's devices by simply including a small receiver coil and circuit in a sleeve attached to the mobile device.

In [44], a three node wireless MIMO broadcasting system for SWIPT is considered, in which two receivers and a single transmitter are involved. In the described scenario, one of the two receiving devices harvests energy from the source, while the other one decodes the transmitted information. Two cases are studied: one in which the information and energy receivers see two different channels from the transmitter, and another one in which they see the same channel. In the first case, optimal transmission strategies to achieve tradeoffs for maximum information rate versus energy transfer are derived. In the second case, instead, a performance bound outside of the rate-energy region is shown. This bound, though, is not reachable with the existing technology, because circuits for harvesting energy from radio signals are not able to also decode information yet.

In [26], the authors equip the secondary users of a cognitive radio network with RF harvesting technology, thus building an RF-powered cognitive radio network. With this approach both spectrum and energy efficiencies are reached, by respectively exploiting cognitive networks and RF harvesting. A dynamic channel selection problem in a multi-channel scenario, especially focusing on the tradeoff between spectrum sensing, data transmission and RF energy harvesting is considered. In this situation, secondary users of the network can harvest en-

ergy for data transmission while the channel is occupied by primary users, that are sending information through it. Following this approach, RF energy harvesting reveals to be a promising technique to sustain the operation of secondary users in RF-powered cognitive radio networks. The problem can also be formulated considering dedicated RF energy sources, in which the secondary users can decide whether to buy energy from the dedicated sources, or to freely harvest it from the transmission of nearby primary users.

In [25], resource allocation issues in wireless networks with RF energy harvesting capability are discussed. A QoS-aware operation policy with service differentiation is also designed for the receiver. Furthermore, an optimal operation policy, that maximises the throughput of a mobile node with RF harvesting technology and achieves service differentiation among different types of data and with packet loss assumption, is obtained.

In [40], the principles and requirements for powering a WSN with RF energy harvesting are discussed, highlighting that this technique is preferred for powering small-sized sensors, such as those that can be found in future Smart Buildings. The power is transmitted in the Industrial, Scientific and Medical (ISM) band, respecting the power constraints imposed by international laws, e.g., those reported in Table 2. The propagation channel is also discussed and it is observed that indoors LoS environments present a better attenuation than free-space ones. Smart Illumination and Li-Fi techniques [30, 37] are also exploited to obtain a better power decay than that predicted by the Friis formula, shown in Equation 7.

In [39], the author studies a tradeoff between the rates at which energy and information can be transmitted over a wireless channel affected by noise. A capacity-energy function of the channel is also found. According to the article, by adopting the found tradeoff, it is possible to receive both large amounts of energy and information per unit of time.

In [19], the authors wirelessly transfer power between a pair of devices by adopting self-resonant coils in a strongly coupled regime. The efficiency of the nonradiative transfer is demonstrated over higher distances than the radii of the two coils. By using this technique, $60W$ were transferred with an efficiency of about 40% across distances of 2m. A quantitative model, describing the wireless power transfer, is also presented and the practical applicability of the system is discussed. Although the reported experiments were run using identical coils, the

receiver's one, i.e., the one inside the portable device, can be made small enough to fit into today's smartphones, or inside their cover, without decreasing the transfer efficiency. In this article it is also highlighted that specific materials and more elaborated geometries can be taken into account in order to improve the transfer efficiency. Also, the described system and technology can already be implemented in today's practical applications.

In [28], an amplify-and-forward relay network is considered. An energy constrained relay node harvests energy from an acquired RF signal and uses it to forward the received information from the source to the destination. Two protocols are considered to enable energy harvesting and information processing at the relay node: a time switching-based relaying protocol and a power splitting-based one. In order to determine the achievable throughput at the destination, an expression for the outage probability is derived for the delay-limited transmission mode, and a formula for the ergodic capacity is found for the delay-tolerant one. From the presented results it emerges that the time switching-based relaying protocol outperforms the power splitting-based one in terms of throughput at low Signal-to-Noise-Ratios (SNRs) and high transmission rate.

In [27], a framework to characterise the charging behaviour of a device that harvests energy from wireless RF signals is designed. Charging equations to replenish energy-depleted storage elements are developed and the charging time distribution, as a function of a given residual voltage distribution, is also derived. Node charging time distribution is derived for uniform and truncated normal distributed residual voltages and shows that the charging time distribution does not always follow the underlying residual voltage distribution. Thanks to the analysis and observations contained in this article, it is possible to appreciate the ability of wireless RF harvesting assisted network operation.

In [29], wireless RF energy transfer is evaluated through a game theoretic approach. The considered network involves a an access point that can transfer energy to the nodes through the wireless channel and, then, they use the harvested energy to transmit their packets. The nodes can send requests, seen as bids, to the access point asking to be charged. The access point adopts an auction mechanism for the wireless energy transfer and the whole game is formulated as a noncooperative game, meaning that the nodes, seen as players, are selfish, do not co-

operate with one another and are only interested in their own outcome. The Nash equilibrium is shown to be a solution of the game and the players try to reach it by using rational strategies and dynamically adapting them during the game. The whole process is also analysed through a Markov chain to study the convergence properties of the game. Finally, as one would expect, it emerges that the Nash equilibrium depends on the cost parameter set by the access point to transmit energy to the nodes.

In [34], the author proposes to place WPT technology inside a user's car to charge a portable device while its owner is driving. This idea is justified by the fact that an average US driver spends 55 minutes a day in its vehicle and that today's mobile devices take, on average, 2 hours to fully charge their battery. The approach followed in this article, thus, does not focus on completely charging the user's device, but to help it being operational for an extra time by steadily replenishing its battery throughout the day. This could be done, for instance, by placing a transmitter coil under the driver's seat and another one attached to the device, for instance embedded in its cover and letting the wireless technology do the rest. The energy to charge the device's battery is provided by the car battery. This method, though, performs worse than [32] and also presents several complications that render the whole system difficult to build. Some of these are the low transfer efficiency of the used coils at the fixed distance seat-user pocket, their inductance and resistance values at the provided frequency and the need of a DC/AC converter, necessary to use the car battery energy to charge the user's device.

In [9, 10], the downlink power transfer and the uplink information one of K-tier Heterogeneous Cellular Networks (HCNs) are studied. In the considered scenario, base stations and energy constrained mobile terminals are randomly located inside the network. Each device pairs up with its corresponding base station, which provides it with the maximum received power. A mobile terminal can harvest energy both from the serving base station, by direct beamforming, and from the other interfering ones. It, then, uses the collected power to send uplink information. Expressions for the maximum transmit power at the mobile terminals and the uplink outage probability and average ergodic rate per terminal are evaluated. Also, asymptotic expressions for the maximum transmit power as the number of antennas goes to infinity are computed. Results show that the

outage probability decreases with an increase of the time allocation for the downlink and that the outage probability and the average ergodic rate per mobile terminal can be improved with the use of massive antenna arrays at the base stations. They also show that the maximum transmit power at the devices can be improved by using a greater number of picocell base stations and that WPT is very efficient in powering the uplink information transmission.

In [1], the authors develop a model for joint uplink and downlink transmission of K-tier HCNs with SWIPT for efficient spectrum and energy utilisation. In the downlink transmission, the mobile users, that are equipped with power splitting receiver architecture, simultaneously decode the received information and harvest energy, while during the uplink transmission, they use the collected energy to transmit information. All the measurements are made by evaluating the performance of a random mobile terminal of the network with the nearest base station to it. The outage probability and the average ergodic rate, both in the downlink and uplink transmission, are evaluated. The presented results show that by increasing the density of the network, the transmit power, the time allocation factor and the energy conversion efficiency of the base stations, the performance of the whole system is not largely affected. However, the uplink performance of a random mobile terminal can be improved by harvesting a larger fraction of the downlink received power.

In [11], the authors introduce a new mathematical approach for the analysis and optimization of cellular-enabled and energy constrained mobile devices with SWIPT. The proposed model represents the locations of the base stations in the network as points of a spatial Poisson point process and exploits stochastic geometry to analyse the system. A channel model, that accounts for LoS and non-LoS links, different cell association criteria, receivers based on time switching and power splitting schemes and directional beamforming is included, too. In this article, again, the results show that a network densification enhances the overall system behaviour. The performance of the model is also increased by increasing the beamforming gain, because this pushes the network to operate close to the noise-limited regime.

In [38], optimization and system level analysis of densely deployed MIMO cellular networks are carried out. In the studied scenario, low-energy devices can both decode information

and harvest energy from the signal received from the base stations, thus dealing with a SWIPT kind of network. The base stations are deployed according to a Poisson point process and the tradeoff between received information rate and harvested power is found by exploiting stochastic geometry tools. Results show that the use of multiple antennas permits to simultaneously increase the information rate and the energy harvested by the nodes.

In [35], a SWIPT technique in a Multiple Input Single Output (MISO) HCN is considered. A femtocell base station sends information to decode and energy to harvest to the UEs. It also suppresses its interference to near macrocell users. Both the information transfer efficiency and energy harvesting efficiency of the femto users are maximised by adopting a fractional programming approach. To study the above problem, a zero-forcing beamformer and a mixed beamforming one are designed and an algorithm to obtain the optimal power with both of them is proposed. Experimental results show that, with the mixed beamforming, better information transfer efficiency and energy harvesting efficiency than with the zero-forcing one are obtained. Moreover, a tradeoff exists between these two metrics.

In [2], the authors study RF energy harvesting from multiple sources in wireless fading channels. As one would expect, the total received power at the antennas of the harvesting nodes changes with the number of the RF source nodes and channel conditions. Moreover, the variation of the instantaneous received power and of the modulation type also affect the time required to recharge a node's battery. Results show that the battery charging time is inversely proportional to the total received power at the node.

In [14], WPT and max data flow problem in rechargeable WSNs are considered. The authors propose to improve the charging rate of some of the network nodes by using auxiliary chargers equipped with WPT technology. Three different solutions, formulated as a mixed integer linear programming problem, are taken into account. In the first one the nodes to upgrade are those on the shortest path from sources to sinks. The second one, instead, starts following the same approach of the first solution and then looks for neighbour nodes yielding a higher max flow. In the third solution Lagrangian and sub-gradient optimization are used to approximate the formulated mixed integer linear programming problem. The second solution re-

veals to be the one with the best performance and the highest max flow rate.

In [22], the authors use near-field capacitively coupled resonators to wirelessly transfer power from a dock charging station to the corresponding device. The designed system consists of a 3D transmitting dock resonator and a receiving circuit board resonator. The transmitting dock uses a ring-shaped metal plate and is specifically designed for the receiving multiband folded-monopole resonator. The smartphone antenna is directly used as the receiving resonator, meaning that the proposed scheme is already implementable in real-world applications.

In [3], magnetic resonant coupling to perform WPT is studied and the authors focus on designing an optimal and high efficiency resonating system. This is composed of an amplifier, coupling coils and a rectifier. The parameters to maintain a high transfer efficiency with respect to distance and load variations are investigated, also taking into account parasitic resistances of the coils and inductor for more accurate results.

In [6], Blanco et al. investigate the RF/DC conversion efficiency of an RF energy harvesting circuit when a digitally modulated signal is received. To run the simulations, signals with the same average power, but with different complementary cumulative distribution function and peak-to-average-power ratio properties are applied at the input of an Ultra High Frequency (UHF) rectifier circuit, optimized to maximise the efficiency under low average input power. The RF/DC conversion efficiency for different loads is also studied and it is shown to depend on the modulation rate used. Results show that an optimum load, which leads to a maximum efficiency, exists and that it depends on the complementary cumulative distribution function and on the peak-to-average-power ratio properties. More specifically, it increases with the increase of the latter metric.

In [8], the authors present a WSN based on UHF RFID technology. This is composed of an interrogator, a sensor tag and a RF energy harvesting system used to power the tag. Each sensor tag is, thus, able to acquire and transmit environmental measurements to the interrogator without using batteries, but exploiting the harvested energy to do it. The maximum distance from the interrogator is up to 5m, assuming a non-continuous acquisition rate, and up to 2m, under a high data rate continuous acquisition. The harvesting efficiency of the designed system can be improved by adapting the reception

antenna to the metallic environment and it is also able to work with other harvesting systems, such as solar panels or vibration transducers.

In [43], a reconfigurable rectifier with adjustable conversion ratio for RF energy harvesting in WSNs is presented. By adopting it, a Wireless Local Area Network (WLAN) RF energy harvesting system, working at the 2.4GHz frequency, with maximum power point tracking is proposed. Results show that the reconfigurable rectifier achieves a high energy harvesting efficiency for a wide available power range and that its response time is over three times lower than that of already existent rectifiers.

In [33], the author examines the possibility for wireless devices to harvest out-of-band RF energy. The general idea of this article is to collect this kind of energy into multi-antenna and single-antenna systems, or simpler devices, such as wireless sensor nodes. A practical architecture, using a 3 port out-of-band RF harvester to permit the opportunistic capture of ambient RF energy, is also designed. Experimental results show that significant portions of ambient energy remain untapped and that these can be harvested using the proposed scheme.

In [36], WPT in energy limited cognitive relay networks is considered. In the studied scenario, a secondary transmitter forwards the traffic from a primary one to a primary receiver, in exchange for serving its own secondary receiver in the same frequency. The secondary transmitter, which employs multiple antennas, is energy constrained and powered by both the energy harvested from the information sent by the primary transmitter and by the energy it harvests from dedicated energy streams, such as the primary and the secondary receivers, that are the final destinations of the sent information packets. This scheme is called destination-aided WPT. The whole system is designed to maximise the rate of secondary users under the energy constraint and the constraint that the required rate of the primary users has to be satisfied. The global optimal solution is derived for the perfect channel state information case, by adopting semi-definite relax technique and Charnes-Cooper transformation. In order to reduce the problem complexity, a suboptimal solution is also found, by adopting matrix decomposition, zero-forcing scheme and dual method. In the imperfect channel state information, convex optimization techniques are exploited to turn the worst case robust problem into a tractable semi-definite one. Results show that the proposed

scheme behaves well in both the perfect and imperfect channel state information cases when the secondary transmitter is relatively close to one of the two receivers.

2.3 CONSIDERED SCENARIO

Contrary to what traditionally done in the literature, for instance in [18, 21, 41], where the nodes do not move in the network and a WCV, or a MC, reaches them to replenish their battery, or in [13], where a MC reaches slowly moving robotic devices to charge them, in our work we considered users travelling along paths that are independent of other users' ones. They move in a network in which a certain number of base stations has already been deployed to relay information from and to the devices and to ensure the correct operation of a telecommunication system.

We assume that the UEs's battery continues discharging in time, either being the related user in motion or not, and that a device is never shut down, nor put on standby, unless its battery discharges completely, in which case the UE is considered *dead* and cannot be wirelessly charged anymore, but needs to be plugged into the power grid. This last case, in which the UE needs to be connected to an electrical source, is not of our concern and a device who dies is no longer considered in our model.

When the energy contained in the UE's battery goes below a certain level, the UE asks the surrounding base stations to be wirelessly charged, possibly paying a certain fee in a real-world scenario. Upon receiving a charging request, a base stations decides whether to charge the requiring device, or not, taking into account different factors, such as the residual battery level of the device, its distance from the base station or the number of energy-requiring devices inside the base station's coverage area. In fact, because omnidirectional antennas are employed in the charging operations and that power is equally transmitted in a spheric area, from a transfer efficiency point of view, it is more convenient to charge multiple devices at once, instead of wasting power to transmit energy to a single requiring one. Single-node charging, though, is still possible, for instance if the requiring-device has a critically low energy level and is about to run out of battery, or, in a real-world scenario, by paying a higher price.

3

MATHEMATICAL MODELS

We will now describe the mathematical models we used. The network model, i.e., the simulation field we considered, is discussed in Section 3.1. An observation of the network status is periodically made in different instants of time, also called *rounds*, thus considering a slotted time system. To complete the simulation, $R \in \mathbb{Z}$ rounds are run, each one of them lasting ΔT seconds.

For the UEs, i.e., the devices in the network, to change their position, we consider the mobility models described in Section 3.2 and enable the various nodes of the network to update their position at each round $r \in [0, R-1]$, where $r = 0$ is the starting round, when the simulation parameters are initialised.

Furthermore, at each round, the battery of the nodes discharges of a certain quantity, and the UEs possibly ask the base stations to be charged, as described in Section 3.3. After receiving charging requests from the nodes, the base stations decide whether to charge of the UEs or not, based on the policies described in Section 3.4.

Finally, some observed metrics are reported in Section 3.5 and the complexity of the control part of the algorithm is discussed in Section 3.6.

3.1 NETWORK

To simulate the network we define our field as a $M_1 \times M_2$ toroidal matrix, with $M_1, M_2 \in \mathbb{Z}$. We randomly deploy N nodes in the network, that represent the UEs and call $\mathbf{n}$ the nodes' vector:

$$\mathbf{n} = [n_0, \ldots, n_{N-1}] \tag{9}$$

We, then, randomly distribute B base stations, with $B \ll N$ and call $\mathbf{bs}$ the base stations' vector:

$$\mathbf{bs} = [bs_0, \ldots, bs_{B-1}] \tag{10}$$

Each base station bs_i, $i \in [0, B-1]$, keeps a list of the nodes that are inside its coverage area A_{bs_i} and each node n_j, $j \in [0, N-1]$, keeps track of all the base stations it can hear from and, in particular, of the nearest one, i.e., the one associated with the highest Received Signal Strength Indicator (RSSI).

3.2 MOBILITY MODELS

In this section we will describe the considered mobility models for the nodes to update their position during each round of the simulation.

We consider the Random Waypoint Mobility Model in Section 3.2.1, the Reference Point Group Mobility Model in Section 3.2.2 and the Manhattan Mobility Model in Section 3.2.3.

3.2.1 *Random Waypoint Mobility Model*

The Random Waypoint Mobility Model permits the UEs to move freely and without restrictions around the network. In this model, first proposed by Johnson and Maltz [7, 17], nodes randomly choose their destination, speed and travelling direction independently of other ones. This mobility model permits to study scenarios in which the users travel alone.

At the beginning of the algorithm each device randomly selects one location in the simulation field as its destination. Then, it uniformly chooses a speed $v \in [0, V_{max}]$, measured in number of cells per round the node can travel. At this point, the user chooses the movement direction in order to get closer to the intended destination.

When the node reaches its destination, it stops for a pause time $T_{pause} \in \mathbb{Z}$, i.e., the number of rounds it does not change position, and then randomly chooses another destination and the whole process repeats until the simulation ends. A correct choice of the pause time in the simulation is of paramount importance [4]: a low T_{pause} leads to a highly dynamic model, while a high T_{pause} leads to a rather static one.

An example of the movement path of a node is shown in Figure 3.

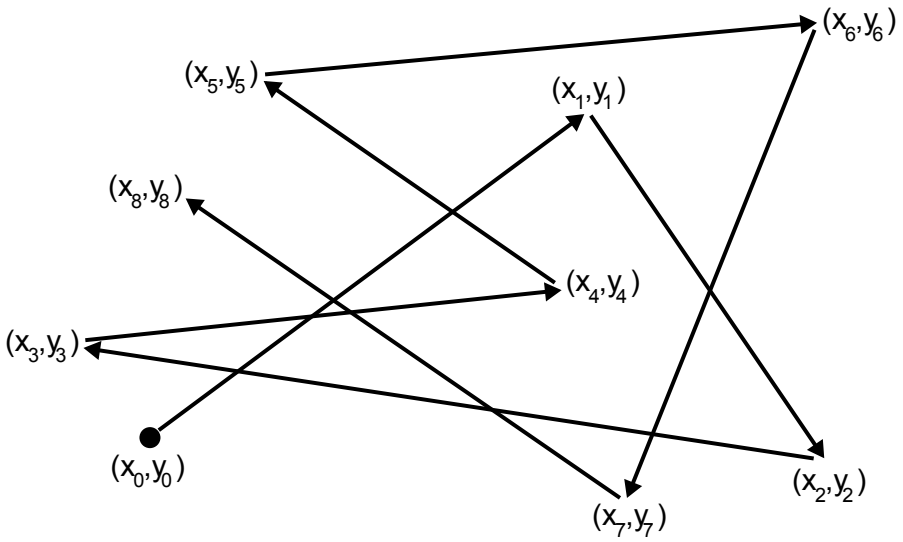

Figure 3: Example of node movement in the Random Waypoint Mobility Model, from [4]. (x_i, y_i), $i \in [1, 8]$, are the different destinations, (x_0, y_0) is the initial position of the node.

3.2.2 *Reference Point Group Mobility Model*

The Reference Point Group Mobility Model [4], contrary to the Random Waypoint model, permits to study the behaviour of nodes whose movements present a spatial dependency, i.e., the nodes move in groups. This model captures more realistic mobility scenarios than the ones considered by random models, for instance, situations in which UEs form teams to work together, or simply users using the public transport network.

In this model nodes are divided into *group leaders* and *followers* and each group is composed of a group leader, that determines the direction of movement and speed of the whole group, and a certain number of followers, that tag along the leader of their group.

At the beginning of the algorithm, each group leader randomly chooses its destination in the simulation field and its speed $v \in [0, V_{max}]$. At each subsequent round, the leader moves to an intermediate location to get closer to its intended destination. The followers, instead, move in the same direction and speed of their group leader, eventually deviating of a bounded number of cells from their reference point, i.e., the point they would reach travelling along the very same direction of their leader and with the same speed. This process goes on until the leader reaches its intended destination, then the whole group stops for a pause time, T_{pause}, after which the

leader chooses another destination and the whole process repeats again.

An example of a group's movement in the Reference Point Group model can be seen in Figure 4.

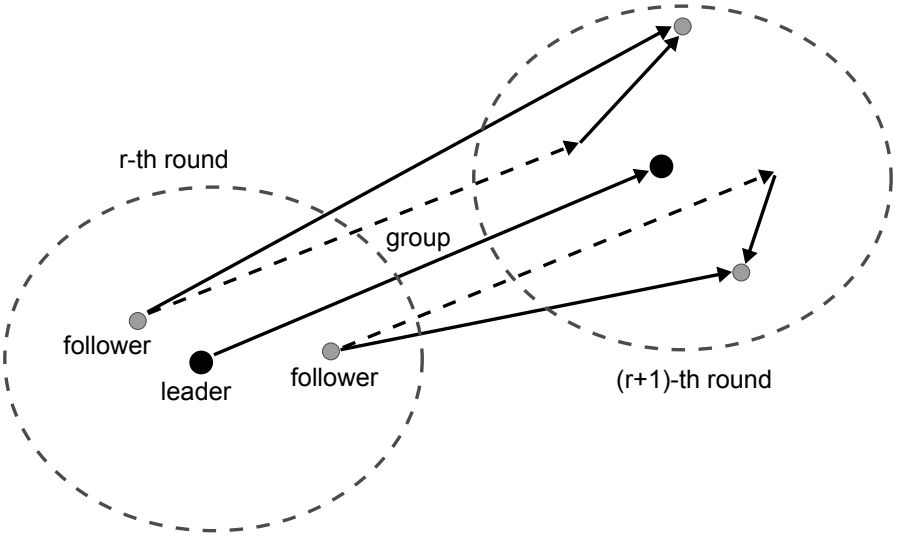

Figure 4: Example of group movement in the Reference Point Group Mobility Model, from [4]. The dashed straight lines represent the followers' reference path in absence of deviations. Two snapshots are given: one at the r-th round, in the left circle, and one at the $(r+1)$-th round, in the right circle.

One key parameter in this model, other than the pause time for the same reasons exposed in Section 3.2.1, is the number of members belonging to the same group, G_{el}. On one hand, if $G_{el} \gg 1$, we have many nodes moving together that enter or exit from the coverage area of the base stations in the same instant, or in consecutive ones. Doing this, they greatly affect the number of nodes a base station can charge in a certain round. On the other hand, if $G_{el} = 1$, each node is a group leader and chooses its own destination independently from that of the other nodes, from which it moves in an autonomous way. In this latter case, each node behaves as if it were in the Random Waypoint Mobility Model.

3.2.3 *Manhattan Mobility Model*

The Manhattan Mobility Model simulates the movement of nodes across streets defined by maps, thus imposing *geographic restrictions* and a high spatial dependency on the possible paths a node can take. Contrary to the Random Waypoint model,

where nodes move freely in the network, this model permits to study realistic urban applications, where nodes' movement is subject to the surrounding environment [4].

This model, first proposed in [5], uses city maps to limit the possible movements of the users. These are composed of horizontal and vertical streets along which the nodes can travel in both direction. The zones of the network surrounded by a group of crossing streets represent the blocks of an urban area. We chose to build squared blocks and place our base stations in the block zone, close to a crossroad, while nodes are initially placed randomly on streets.

A node currently travelling on a certain street, upon arriving to an intersection with another street, can change direction by turning left or right. More specifically, it continues on the same direction with 0.5 probability, while it turns either left or right with probability equal to 0.25.

Mainly considering pedestrian users, differently to what done in [5], we do not impose a user to have at most the same speed of the one preceding it in its moving direction, but a user's speed, v, is chosen randomly in $[0, V_{max}]$.

Nodes of the network continue moving in this way until the end of the simulation. A possible map for the Manhattan Model is shown in Figure 5.

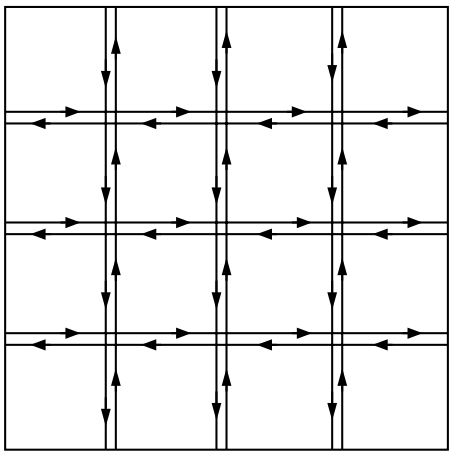

Figure 5: Example of map for the Manhattan Mobility Model, from [5].

An important parameter in this model is the length of the edge of each block, L_b. A low value of L_b leads to a network with a high density of streets and where the nodes' movement is not very limited, while a high one leads to larger blocks and, thus to less streets along with the nodes can travel. Also, plac-

ing the base stations inside buildings, we limit their sensing and charging range to the nearby streets.

3.3 BATTERY DISCHARGE AND CHARGING REQUEST

At each round r the UE's battery discharges with probability $p_{disch} \in [0, 1]$, according to the following model: defining $E_{n,r-1} \in [0, E_{max}]$J the energy contained in node n's battery at round $r-1$, pick a random quantity $E_q \in [1, E_{q,max}]$J and compute the battery energy at round r, i.e., the new energy level after battery discharges, as:

$$E_{n,r} = \begin{cases} E_{n,r-1} - E_q, & \text{if } E_{n,r} > 0 \\ 0, & \text{otherwise} \end{cases} \tag{11}$$

If $E_{n,r} = 0$, i.e., if the battery discharges completely, the node is considered *dead* and it does not participate in the simulation anymore.

When the battery energy level of a node goes below a certain threshold, E_{thr}, the node broadcasts a *charging request* to all the reachable base stations, that receive and store it in a dedicated list. When a node that previously issued a charging request has been charged and its battery level goes above another threshold $E_{safe} > E_{thr}$, it no longer requires energy to the base stations. An *error-free channel* is assumed for the transmission of requests.

3.4 CHARGING POLICIES

Each base station performs a control on the received requests once every $R_{cnt} > 1$ rounds and decides whether to charge, or not, a node inside its coverage area A_{bs} that issued a charging request according to the following charging policies: *Genie Charging Policy*, described in Section 3.4.1, and *Heuristic Charging Policy*, described in Section 3.4.2. If the base station decides to charge, it charges all the energy-requiring nodes inside its coverage area, as discussed in Section 3.4.3.

The frequency in which the control operations are performed is lower than the one in which nodes' movement takes place, i.e., at each round, so that base stations are not overwhelmed with charging-related operations, but can also execute their normal duties, such as relying information from and to the nodes and similar ones.

3.4.1 *Genie Charging Policy*

In the genie charging policy we assume that all the future positions and battery levels of all the nodes in the network at each round are known to the base stations. Each base station considers a window $\mathcal{W}$ of $W \in \mathbb{Z}$ rounds in the future. This is assumed here to come up with a lower bound for the performance that can be achieved by heuristic and practical schemes.

We, then, focus on two different sub-policies: a simplified version of the genie policy and a complete one, as discussed below. This kind of policy is used to draw a reference on the performance of the designed heuristic algorithms, depicted in Section 3.4.2.

Simplified Genie

In this simplified version of the genie policy each base station examines its window $\mathcal{W}$ and computes the number of energy-requiring nodes that will be inside its coverage area in each round $r \in \mathcal{W}$. It selects as starting round to begin the charging process the optimal round $r^* \in \mathcal{W}$ in which its coverage area contains the higher number of nodes needing to be charged. Then, it starts charging all such nodes and continues doing so for a constant number of rounds $\Delta < W$, $\Delta \in \mathbb{Z}$. After this, the base station considers another window $\mathcal{W}$ of W rounds and the process restarts again.

An example of a possible looking window for simplified policies is shown in Figure 6.

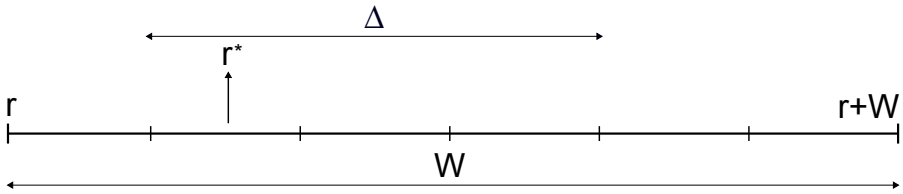

Figure 6: Example of looking window $\mathcal{W}$ for the simplified charging policies.

Complete Genie

In the complete version of the genie policy, instead, each base station cycles through all the possible rounds $r_s \in \mathcal{W}$ in which it can start charging the requiring nodes inside its coverage area A_{bs}. Then, it cycles through all the possible rounds $r_e \in \mathcal{W}$ in

which it can finish the charging process, with $r_e \geqslant r_s$, and it computes the energy efficiency for each pair (r_s, r_e), as:

$$\eta(r_s, r_e) = \sum_{r=r_s}^{r_e} \frac{E_{TX,bs,r}}{\sum_{i=0}^{N-1} E_{RX,n_i,r} \cdot i(n_i) \cdot e(n_i)}, \tag{12}$$

with $\eta(r_s, r_e) \geqslant 1$. $E_{TX,bs,r}$ is the energy related to the power transmitted by base station bs during round r, defined in Equation 25, and $E_{RX,n,r}$ is the energy received by node n during round r, defined in Equation 26. $i(n)$ is an indicator function of whether the node n is inside the coverage area of the base station, or not:

$$i(n) = \begin{cases} 1, & n \in A_{bs} \\ 0, & \text{otherwise} \end{cases}, \tag{13}$$

while $e(n)$ is an indicator function of whether the node n needs to be charged, or not:

$$e(n) = \begin{cases} 1, & n \text{ needs to be charged} \\ 0, & \text{otherwise} \end{cases} \tag{14}$$

An example of a possible looking window for complete policies is shown in Figure 7.

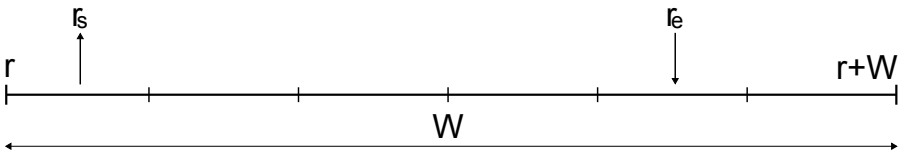

Figure 7: Example of looking window $\mathcal{W}$ for the complete charging policies.

At this point, the base station selects the optimal pair of rounds $(r_s^*, r_e^*) \in \mathcal{W}$ in which to begin and end the charging process in order to minimise the energy efficiency function:

$$\eta(r_s^*, r_e^*) = \min_{r_s, r_e \in \mathcal{W}} \eta(r_s, r_e) \tag{15}$$

3.4.2 *Heuristic Charging Policy*

In the heuristic charging policy the base stations know nothing about the nodes at the beginning of the algorithm. Each base station, given that a node is inside its coverage area A_{bs} and by observing at least two positions of the node, is able to predict its future behaviour in the way we now expose. First, by knowing two positions of a node, for instance, given that we are at round r, the position at round $r-1$, $\mathbf{p}_{n,r-1}$, i.e., the previous one, and $\mathbf{p}_{n,r}$, i.e., the current one, the base station is able to estimate the speed of the node, $\boldsymbol{v}_n$, as:

$$v_{n,x} = \frac{p_{n,r,x} - p_{n,r-1,x}}{\Delta T} \tag{16}$$

$$v_{n,y} = \frac{p_{n,r,y} - p_{n,r-1,y}}{\Delta T}, \tag{17}$$

where ΔT is the length of a round and v_x and v_y are the two components of the speed, represented as follows:

$$\boldsymbol{v} = [v_x, v_y], \tag{18}$$

while p_x and p_y are the two components of the node's position, represented as follows:

$$\mathbf{p} = [p_x, p_y] \tag{19}$$

Then, the base station is able to estimate a possible future location of the node, e.g., the one at round $\hat{r} > r$, $\mathbf{p}_{n,\hat{r}}$, as:

$$p_{n,\hat{r},x} = p_{n,r,x} + v_{n,x} \cdot (\hat{r} - r) \cdot \Delta T \tag{20}$$

$$p_{n,\hat{r},y} = p_{n,r,y} + v_{n,y} \cdot (\hat{r} - r) \cdot \Delta T, \tag{21}$$

where the term $\hat{r} - r$ accounts for the number of rounds to go from the current round r to the future one $\hat{r}$, with each round lasting ΔT seconds.

If base station bs_i, that is estimating the future positions of the nodes inside its coverage area, sees that the estimated future position of a device falls inside another base station's coverage area, e.g., inside the one of base station bs_j, with $i, j \in [0, B-1]$, $i \neq j$, it notifies bs_j of this fact, thus giving it an estimation of its future arrivals. Given that each base station executes the

above computations, an estimation of nodes' future arrivals and departures is given to all base stations of the network.

Each base station, then, considers a window $\mathcal{W}$ of $W \in \mathbb{Z}$ rounds in the future and estimates future departures of the nodes currently inside its coverage area for each round $r \in \mathcal{W}$ and, thanks to the interaction with the other base stations, also receives an estimation of nodes' future arrivals inside its coverage area.

Analogously to what done in Section 3.4.1 for the genie charging policy, we focus on two different sub-policies: a simplified version of the heuristic policy and a complete one, as described below.

Simplified Heuristic

In the simplified version of the heuristic policy each base station considers the current window $\mathcal{W}$ and the estimated locations of the nodes within its coverage area for each round $r \in \mathcal{W}$. Then, it selects as starting round to perform the charge the optimal round $r^* \in \mathcal{W}$ in which more energy-requiring nodes are estimated to be inside its coverage area. After it begins the charging process, the base station continues charging all the energy-requiring nodes it can reach for $\Delta < W$, $\Delta \in \mathbb{Z}$ rounds, with Δ fixed a priori. When this task ends, the base station considers another window $\mathcal{W}$ of W rounds and the described procedure restarts anew. We refer to Figure 6 for an example of looking window for this policy.

Complete Heuristic

In the complete version of the heuristic policy, instead, each base station considers the previously described estimation of future arrivals and departures of energy-requiring nodes in its window $\mathcal{W}$. Then, analogously to what done in Section 3.4.1 for the complete genie policy, it cycles through all the possible pairs of starting and ending charging rounds $(r_s, r_e) \in \mathcal{W}$, with $r_e \geqslant r_s$ and selects the optimal pair of rounds (r_s^*, r_e^*) in order to minimise Equation 12, as done in Equation 15, where Equation 13 is based on the position estimates and Equation 14 on the effective charging requests received by the base station. We refer to Figure 7 for an example of looking window for this policy.

3.4.3 *Power Transfer*

To charge nodes omnidirectional antennas are assumed at the base stations. Denoting with $P_{TX,bs}$ the power transmitted by base station bs, and with $P_{RX,n}(d)$ the one received at node n, we have:

$$P_{RX,n}(d) = P_{TX,bs} \cdot \mu_n(d), \tag{22}$$

where d is the distance between n and bs and $\mu_n(d) \in [0, 1]$ is the power transfer efficiency function between bs and n and is given by:

$$\mu_n(d) = -0.0958 \cdot d^2 - 0.0377 \cdot d + 1 \tag{23}$$

As done in [18], Equation 23 is derived through a curve fitting of experimental measurements on the efficiency of simultaneous wireless power transfer, whose experimental results are reported in [20]. This equation also gives an upper bound on the maximum distance a base station can charge a node, i.e., on the charging radius R_{ch}, in fact we have:

$$\mu_n(d) \geqslant 0 \iff d \leqslant 3.04m \tag{24}$$

Thus, the maximum charging radius is $R_{ch,max} \approx 3.04m$.

The energy related to the power transmitted by base station bs in a single round is given by:

$$E_{TX,bs} = \int_{\Delta T} P_{TX,bs} dt = P_{TX,bs} \cdot \Delta T, \tag{25}$$

where the last equality is due to the fact that the power is transmitted across a constant period of time ΔT, i.e., the duration of a round. The energy related to the power received at node n in the same round is, instead, as follows:

$$E_{RX,n} = \int_{\Delta T} P_{RX,n}(d) dt = P_{RX,n}(d) \cdot \Delta T, \tag{26}$$

where the last equality is due to the fact that the power is received across a constant period of time ΔT.

At the end of the charging process, performed at round r, the energy contained in node n's battery is given by:

$$E_{n,r} = \begin{cases} E_{n,r-1} + E_{RX,n}, & \text{if } E_{n,r} < E_{max} \\ E_{max}, & \text{otherwise} \end{cases} \tag{27}$$

3.5 METRICS

The measured metrics are the total energy associated with the power transmitted by the base stations and the total one received by all the nodes throughout the R rounds of the simulation, respectively given by:

$$E_{TX}(tot) = \sum_{r=0}^{R-1} \sum_{i=0}^{B-1} E_{TX,bs_i,r} \tag{28}$$

$$E_{RX}(tot) = \sum_{r=0}^{R-1} \sum_{i=0}^{N-1} E_{RX,n_i,r} \tag{29}$$

We want to minimise the ratio between Equation 29 and Equation 28, i.e., the total energy efficiency function, defined as:

$$\eta_{tot} = \frac{E_{TX}(tot)}{E_{RX}(tot)} \tag{30}$$

with $\eta_{tot} \geqslant 1$. We measure the fraction of dead nodes at the end of the simulation, i.e., at the beginning of the *virtual* round $r = R$, given by:

$$F_{dn,tot}(N) = \frac{N_{dn}(R)}{N} \tag{31}$$

where $N_{dn}(r)$ is the number of dead nodes at round r and $F_{dn,tot}(N) \in [0, 1]$. We also compute the number of dead nodes as a function of the rounds, as:

$$F_{dn}(r, N) = \frac{N_{dn}(r)}{N} \tag{32}$$

We, then, measure the average battery level of the nodes per round:

$$B_{avg}(r, N) = \frac{1}{N} \sum_{i=0}^{N-1} \frac{E_{i,r}}{E_{max}} \tag{33}$$

where $B_{avg}(r, N) \in [0, 100]$.

3.6 COMPLEXITY OF HEURISTIC POLICIES

In a real-world scenario, the greatest burden a base station has to cope with in the control part of the described algorithm is represented by the adopted charging policy.

In both the heuristics we considered in Section 3.4.2, a base station first has to estimate the future departures of the nodes currently inside its coverage area. This estimation requires the following number of operations:

$$\sum_{i=0}^{N-1} i(n_i) = \mathcal{O}(N_{ins}) \tag{34}$$

where N_{ins} is the number of nodes inside the base station's coverage area. Thus, the complexity of this first passage grows linearly with the number of inside nodes. The estimation of the future arrivals, instead, comes for free, because they are notified by the other base stations.

In the simplified heuristic policy, then, a base station considers a window of W rounds in the future and finds the round with the greatest number of nodes inside its coverage area. This part requires to go through each of the W rounds of the window $\mathcal{W}$ and, thus, requires $\mathcal{O}(W)$ operations. Finally, the base station charges the nodes for a constant number Δ of rounds. A possible looking window for this policy is shown in Figure 6.

In the complete heuristic charging policy, instead, the heaviest operation a base station has to perform, after going through the previously depicted estimation, is the energy efficiency function minimisation, made through Equation 15. The base station considers a looking window $\mathcal{W}$ of W rounds in the future and has to compute the energy efficiency function, $\eta(r_s, r_e)$, reported in Equation 12, for all the possible rounds $(r_s, r_e) \in \mathcal{W}$.

The starting round r_s can be chosen independently in W different ways, while the choice of the ending round r_e depends on the particular value of r_s we picked, in fact the restriction $r_e \geqslant r_s$ holds. Given that we are at round r, for instance, we can freely pick r_s among all the possible W values of the considered looking window $\mathcal{W}$, and, once we fixed it, we can choose r_e among the remaining $r + W - r_s + 1$ values belonging to the

same window. In the above expression, $r + W - r_s$ is the number of rounds in the window from r_s, excluded, to the end of the window, i.e., to round $r + W$, and the summed extra round accounts for the fact that it can be $r_e = r_s$, thus starting and ending the charging process in the same round, i.e., performing the charging operation in a single round. A possible looking window for this policy is shown in Figure 7.

The total number of operations required to perform the minimisation is:

$$\sum_{i=0}^{W-1} (W - i) = \sum_{i=0}^{W-1} W - \sum_{i=0}^{W-1} i = W^2 - \frac{(W-1) \cdot W}{2} = \mathcal{O}(W^2) \tag{35}$$

To sum up, the complexity of the simplified heuristic policy is $\mathcal{O}(N_{ins} + W)$, while that of the complete heuristic policy is $\mathcal{O}(N_{ins} + W^2)$.

Following a similar reasoning for the considered genie charging policies, and given that no estimation of future arrivals and departures is needed, the complexity of the simplified genie policy is $\mathcal{O}(W)$, while that of the complete genie policy is $\mathcal{O}(W^2)$. We are not very interested, though, in the complexity of the genie policies, because, as stated above, these policies are considered with the only purpose of giving a reference for heuristic policies and are not appropriate for an online use.

4

SELECTED RESULTS

In this chapter, we present some of the results obtained from the experiments we ran. In order to simulate the network and get these results, we wrote a code in C language and performed a number of simulations using a MacBook Pro computer with OS X 10.11 and a 2.5GHz Intel Core i7 processor.

We considered two different scenarios: one with Normal Mobility (NM), in Section 4.1, accounting for pedestrian users, in which $V_{max} = 2.8m/s$, and another with Fast Mobility (FM), in Section 4.2, accounting for driving users, in which $V_{max} = 30km/h$.

The values for the parameters used in the experiments are shown in Table 3.

In both the studied scenarios, we measured the total energy efficiency η_{tot}, given in Equation 30, the fraction of dead nodes at the end of the simulation, $F_{dn,tot}(N)$, as shown in Equation 31, the number of dead nodes as a function of the round, $F_{dn}(r, N)$, as reported in Equation 32, the average battery level per round, $B_{avg}(r, N)$ as shown in Equation 33, and the total energy transmitted by the base stations, $E_{TX}(tot)$, i.e., the one related to the total transmitted power, as shown in Equation 28, for the three implemented mobility models.

4.1 NORMAL MOBILITY SCENARIO

In this scenario, the maximum speed for the users to move is $V_{max} = 14$ cells/round, i.e., $2.8m/s$, and the average user's speed equals $1.4m/s$, that is the average speed of a walking human being. This scenario, in facts, considers pedestrian users.

4.1.1 *Total Energy Efficiency*

Here we discuss the results regarding the total energy efficiency η_{tot}, reported in Equation 30. We recall that, although usually higher values are better for a function whose name is efficiency, in this case, lower ones are preferred, because it means that the power transmitted by a base station, and thus its corresponding

Parameter	Experiment Value	SI Value
B	3 base stations	3 base stations
E_{max}	1500J	1500J
$E_{q,max}$	2J	2J
E_{safe}	$50\% \cdot E_{max}$	750J
E_{thr}	$30\% \cdot E_{max}$	450J
G_{el}	2 nodes	2 nodes
L_b	3 cells	3m
M_1, M_2	100 cells	100m
N	$[10, 50]$ nodes	$[10, 50]$ nodes
P_{TX}	$4W$	$4W$
p_{disch}	0.01	0.01
R	6000 rounds	$30000s = 8.33h$
R_{ch}	2.5 cells	2.5m
R_{cnt}	3 rounds	15s
ΔT	5s	5s
T_{pause}	1 round	5s
V_{max}	$\{14, 42\}$ cells/round	$\{2.8m/s, 30km/h\}$
W	6 rounds	30s
Δ	3 rounds	15s

Table 3: Values for the parameters used in the experiments.

energy, is better employed at the nodes, i.e., more energy is used to charge batteries.

Figure 8 shows η_{tot} for different values of N when the Random Waypoint Model (RWP) is applied. As expected, the Simplified Genie Policy (SGP) and Complete Genie Policy (CGP) respectively give lower bounds on the efficiency values of the Simplified Heuristic Policy (SHP) and Complete Heuristic Policy (CHP). CHP is the policy whose efficiency has the highest values, and behaves as SHP when $N = 50$, i.e., its performance improves when more nodes are involved. Looking at SGP, CGP and SHP, we can see that they behave in a similar way, with SGP and CGP respectively being the best policy for $N \leqslant 20$ and $N > 20$. CHP, instead, is the policy presenting the worst performance. This aspect, that will also present using the other mobility models we considered, is due to the fact that it is not so trivial to predict nodes' behaviours and future positions in the network and estimates could be wrong, although, many nodes may be located inside the base station's coverage area anyway.

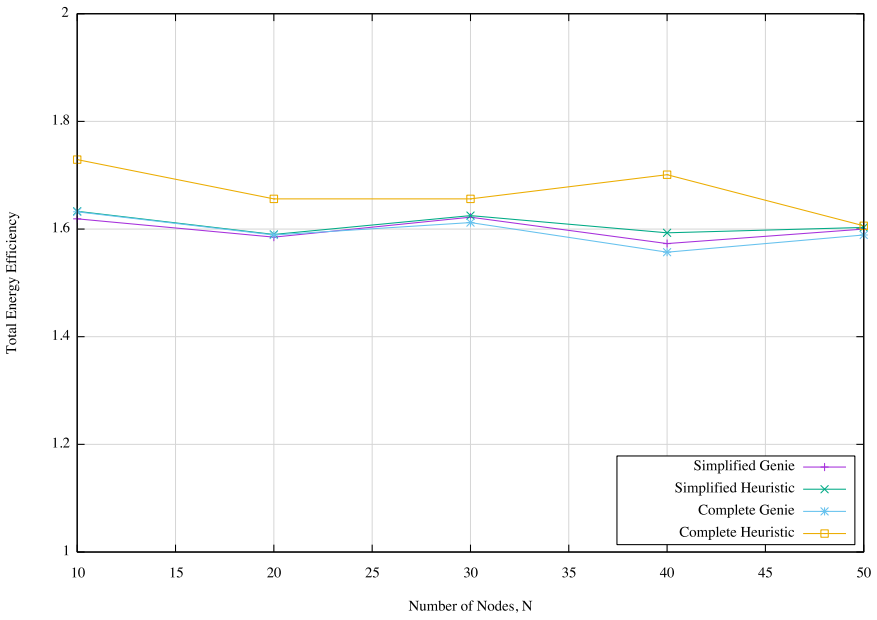

Figure 8: η_{tot} for different values of N: RWP.

Shifting to a more complex movement model, that can be used not only to study cases of groups of people moving together, but also those of single users carrying more devices with them, the Reference Point Group Mobility Model (RPGM), shown in Figure 9, assumes similar behaviours to those presented by RWP. In RPGM, in fact, all the policies present lower, and thus better, efficiency values than the RWP ones. Specif-

ically, the gap between SHP and SGP is broader than the one considering RWP. CHP, as seen in the RWP case, and for the same reasons, generally presents the worst performance. All the other policies present $\eta_{tot} \approx 1.2$ throughout the simulation. This value is very close to the best achievable one, that is $\eta_{tot} = 1$.

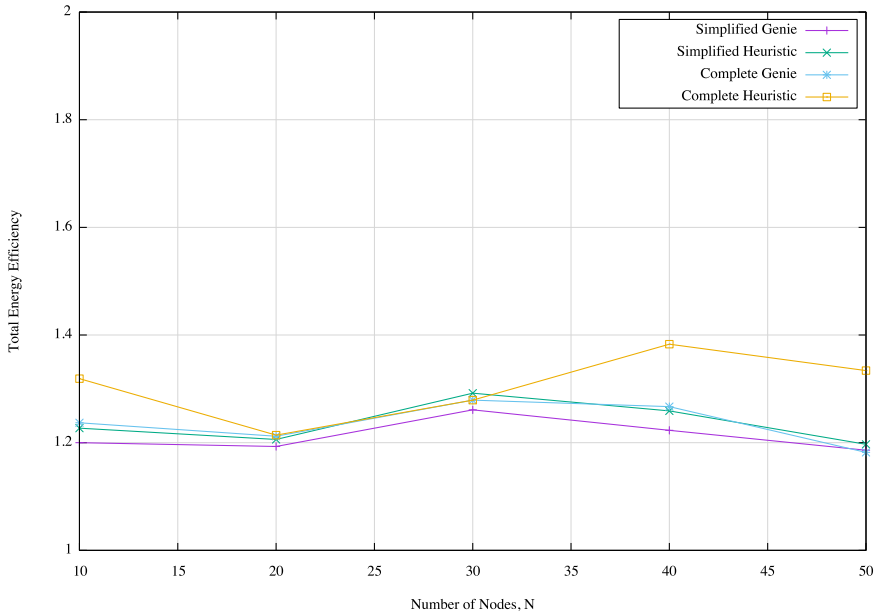

Figure 9: η_{tot} for different values of N: RPGM.

The remarkable aspect is that the efficiencies of RPGM assume surprisingly lower values than the RWP ones, due to the fact that, in RPGM, correlated group movement takes place and more nodes are inside a base station's coverage area, on average.

Figure 10, instead, shows the energy efficiency function when the Manhattan Model (MM) is adopted. In this case, the same considerations made for the RWP experiment of Figure 8 hold, noting that all the policies, but CHP behaves slightly better in MM than in RWP. CHP, instead, maintains higher values than what it does in RWP for $N < 40$, and then reaches lower ones, reaching the other policies, especially SHP. The similar behaviour presented by this model, with respect to the RWP one, shows that, although the possible movements of the nodes are limited by streets and buildings, as one would expect in a real-world urban scenario, the designed policies can cope with these restrictions and the overall result is as good as if we were in free space, or even slightly better.

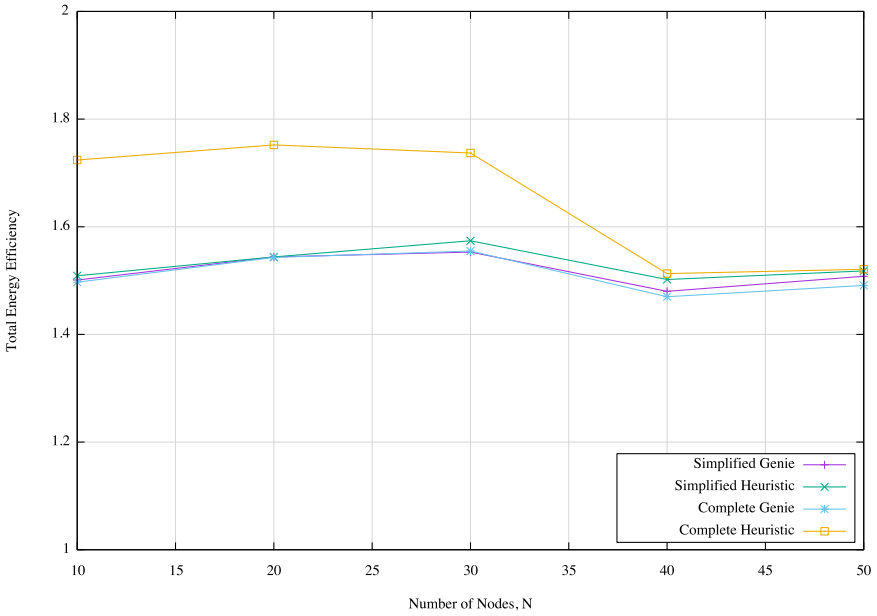

Figure 10: η_{tot} for different values of N: MM.

In Figure 11, we compare the charging policies in the considered motion models. In SGP, SHP and CGP, respectively shown in Figures 11a, 11b and 11c, RWP is the model with the lowest performance, followed by MM and RPGM, that presents the lowest one. In CHP of Figure 11d, instead, MM has worse performance than RWP until $N \approx 33$ nodes, then RWP assumes the worst behaviour of all the three considered mobility models. RPGM, instead, presents the best performance of all. This fact indicates that, even in real-world scenarios, such as that represented by MM, the designed policies behave well, although the group movement, represented by RPGM, always outperforms the other two models.

Finally, Figure 12 shows the comparison of all the efficiency cases discussed so far for all the studied movement models.

To sum up, we see that even with quite simple policies, like SGP and SHP, that charge for a fixed number of rounds Δ, the resulting total energy efficiency η_{tot} reaches values comparable with those of more complex ones, such as CGP. CHP, instead, presents the worst performance of all the designed policies in many of the studies cases.

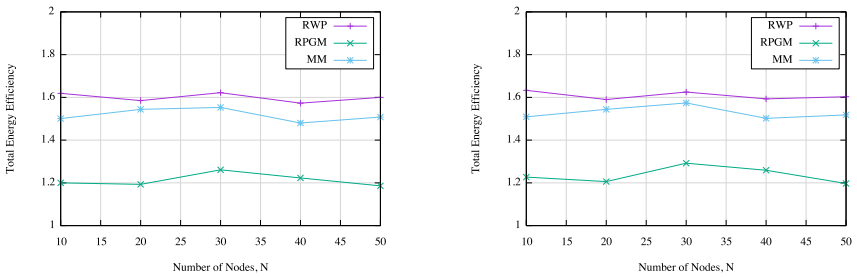

(a) Simplified Genie Policy

(b) Simplified Heuristic Policy

(c) Complete Genie Policy

(d) Complete Heuristic Policy

Figure 11: η_{tot} for different values of N. RWP , RPGM and MM are respectively shown in violet, light blue and green.

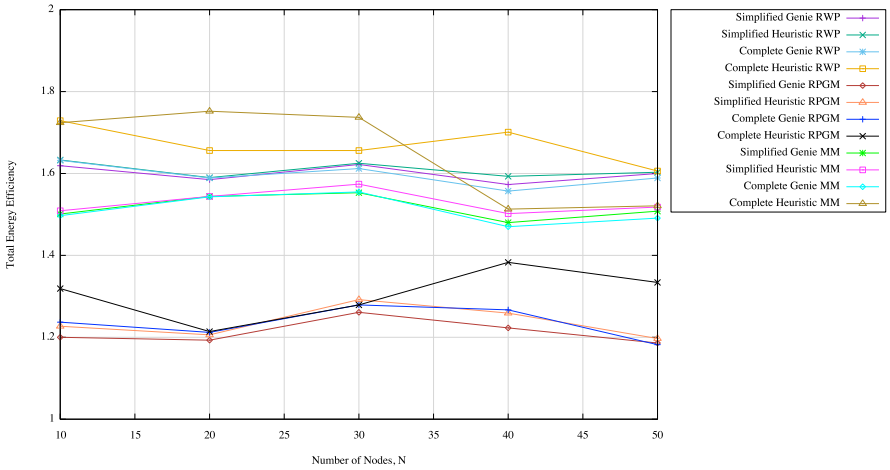

Figure 12: η_{tot} for different values of N: comparison of all policies. RWP, RPGM and MM are shown.

4.1.2 *Fraction of Dead Nodes*

In this section we show the results regarding the fraction of dead nodes at the end of the simulation, $F_{dn,tot}(N)$, reported in Equation 31. Also for this parameter, lower values are preferred, meaning that a higher number of nodes ended the simulation without their battery being exhausted.

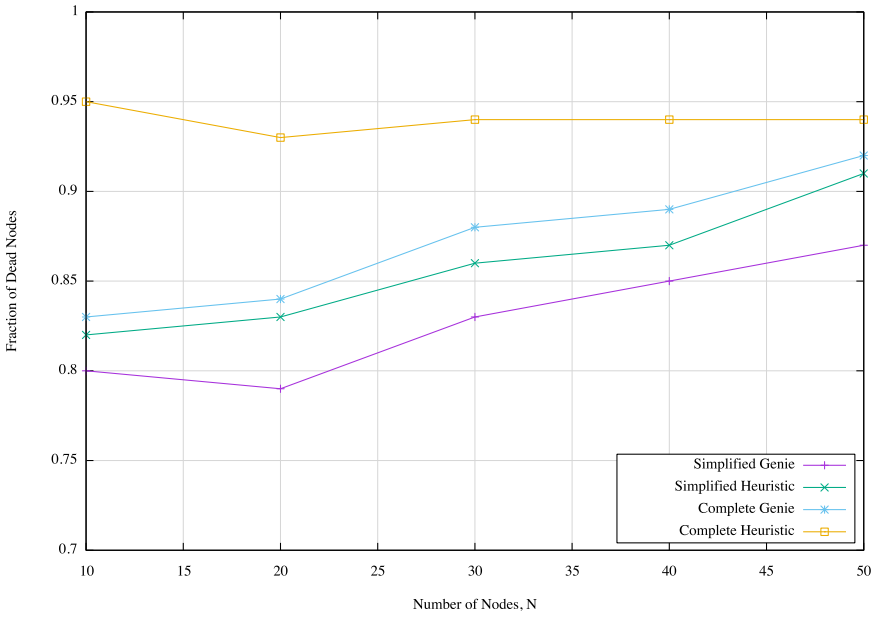

Figure 13: $F_{dn,tot}(N)$ for different values of N: RWP.

Figure 13 presents the results regarding RWP. Looking at this plot, we can say that while SGP, SHP and CGP follow the same behaviour, starting with higher values of dead nodes when $N = 10$, and, then, increasing them as N grows, CHP maintains an almost flat curve. In the latter policy, also being the one presenting the highest number of dead nodes, the curve starts quite high when $N = 10$, and then reaches stable values from $N = 30$ onward, giving us a hint that this policy behaves better when dealing with a large number of users. We can anticipate that this behaviour, in which all the policies almost run in the same way, but CHP, whose curve is much higher than the other ones, will be encountered also using the other mobility models.

In Figure 14, we show the case of RPGM. Similar considerations to those done for Figure 13 hold. In particular we see that all the curves start with lower values than those they present in the RWP case, then they increase, reaching the highest point when $N = 30$ nodes, and, finally, decrease again.

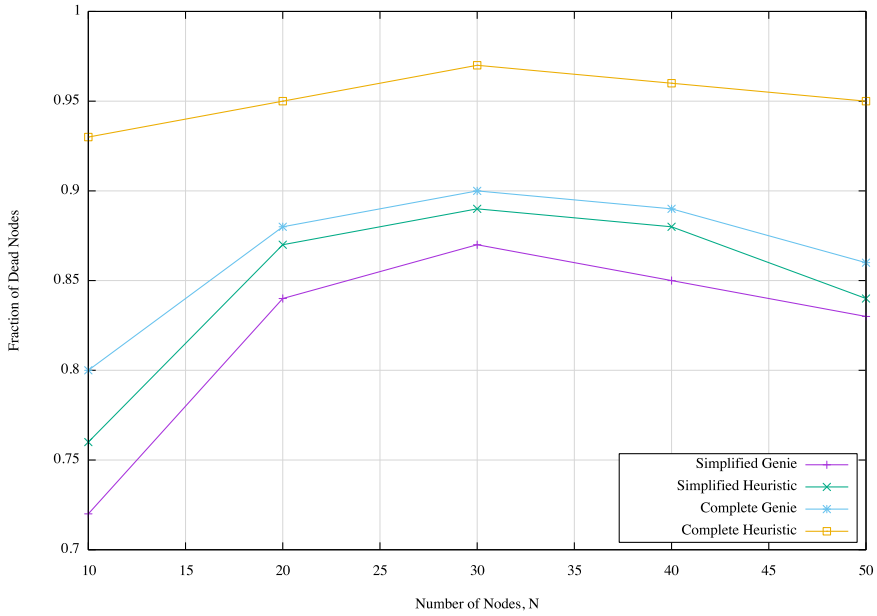

Figure 14: $F_{dn,tot}(N)$ for different values of N: RPGM.

Figure 15 shows the results when MM is used. The same considerations made for Figure 13 hold.

We now analyse the results from the various policies in Figure 16 for the different mobility models we considered. In SGP, SHP and CGP, respectively shown in Figures 16a, 16b and 16c, RPGM is the best mobility model of all when $N = 10$ and when $N = 50$. For values of $N \in [20, 40]$, instead, all the curves intertwine, with MM resulting the best one and RPGM the worst one, when $N = 30$. RWP, instead, behaves well when $N = 20$, but results the worst curve when $N = 50$. All the models, though, present almost the same fraction of dead nodes throughout the simulation. Similar considerations hold in the CHP case of Figure 16d, with the exception that RWP now presents the best curve, when $N = 50$, and both RPGM and MM assume slightly higher values. Also in this case, all the three mobility models behave in a similar way. We can see that all the curves, but the RPGM one, that presents a concave behaviour, generally tend to grow with an increasing N.

Finally, Figure 17 shows the comparison of the results discussed so far on the fraction of dead nodes at the end of the simulation for all the mobility models.

To sum up, we see that, when the simplified policies are used, a lower number of nodes die than when the complete ones are applied. The surprising aspect is the slightly decreasing behaviour CHPs presents, in some cases, with an increasing N.

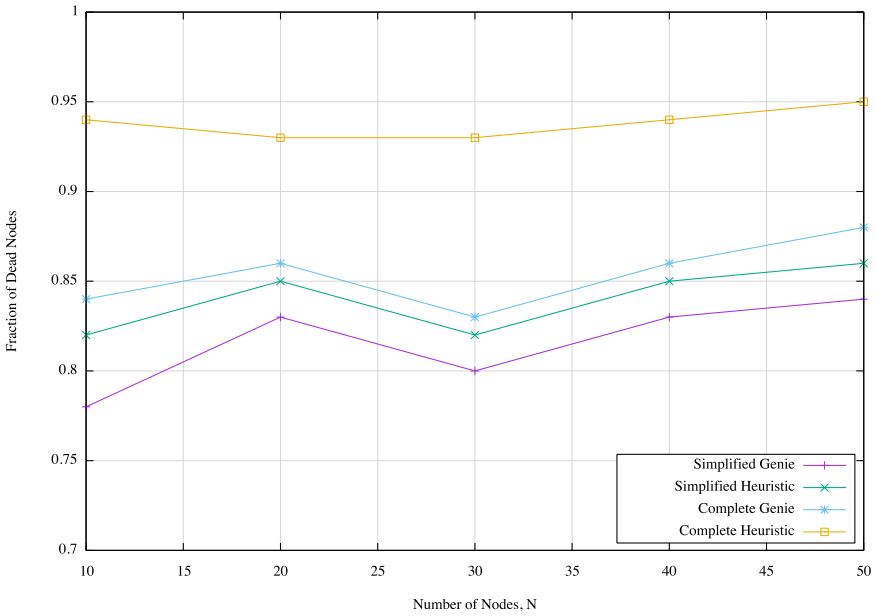

Figure 15: $F_{dn,tot}(N)$ for different values of N: MM.

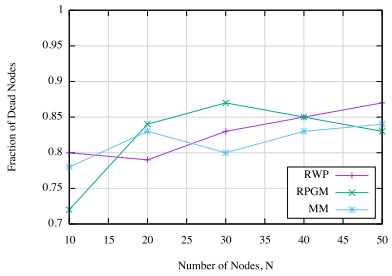

(a) Simplified Genie Policy

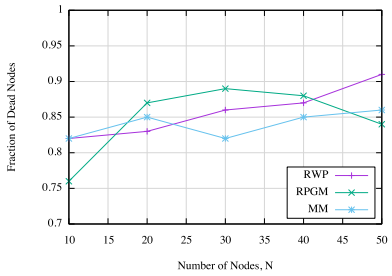

(b) Simplified Heuristic Policy

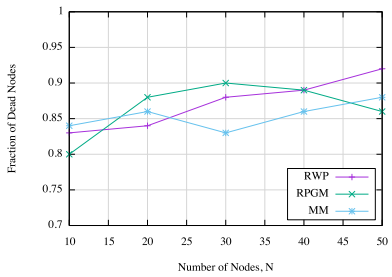

(c) Complete Genie Policy

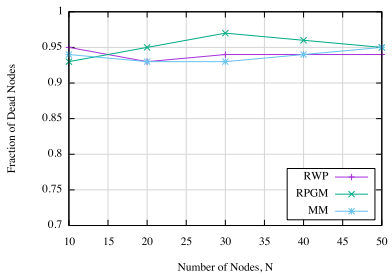

(d) Complete Heuristic Policy

Figure 16: $F_{dn,tot}(N)$ for different values of N. RWP , RPGM and MM are respectively shown in violet, light blue and green.

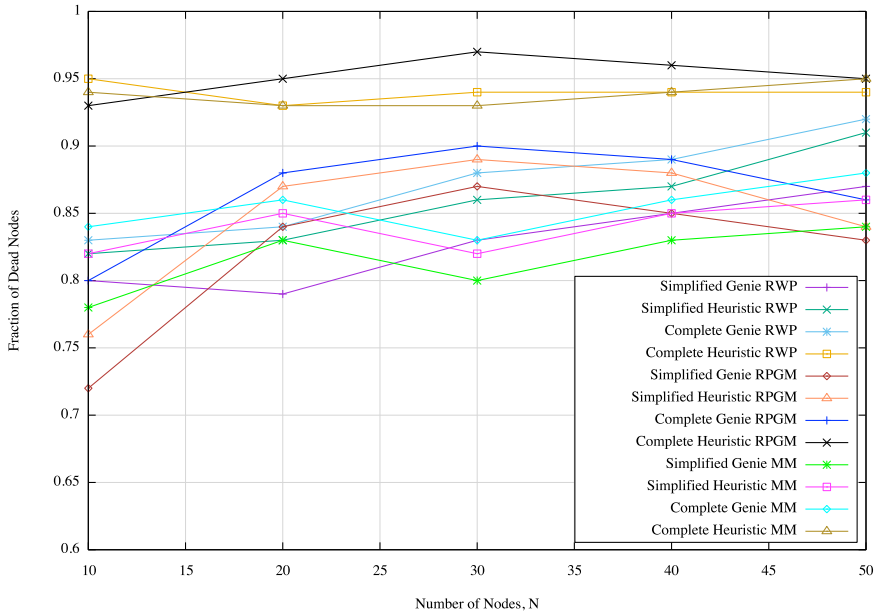

Figure 17: $F_{dn,tot}(N)$ for different values of N: comparison of all policies. RWP, RPGM and MM are shown.

This is probably due to the fact that, even if it is difficult to forecast the future movements of the nodes in the network and wrong estimates are possible, when a high number of nodes is present, some of them will be inside the coverage area of the base station anyway.

4.1.3 *Dead Nodes per Round*

From the results on the fraction of the dead nodes at the end of the simulation, presented in Section 4.1.2, it may seem counterproductive the use of heuristic policies, because of the high number of nodes whose battery completely discharges. It may be interesting, though, to examine how this discharge trend goes on throughout the simulation. For this purpose, in this section we briefly show the results regarding the fraction of dead nodes per round, $F_{dn}(r, N)$, reported in Equation 32, in the experiment with $N = 50$ nodes.

Figure 18 compares this metric for each of the charging policies we considered, when the three mobility models we studied are applied. As we previously saw, SHP and SGP are the policies in which fewer nodes discharge their battery. This is probably due to the fact that they start charging devices in the round in which the base stations have the highest number of nodes inside their charging range and continue doing so for a

fixed number Δ of rounds, regardless of the resulting efficiency. Instead, CGP, and especially CHP, are the ones in which the highest number of nodes die.

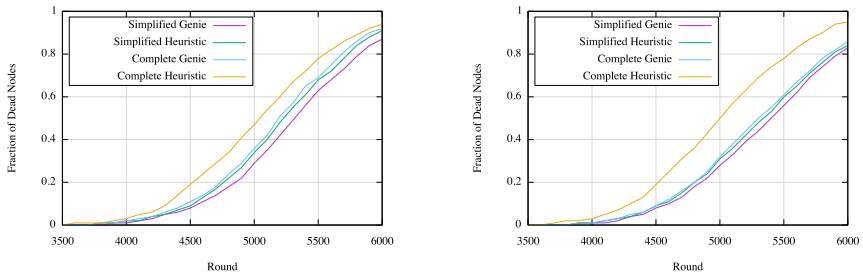

(a) RWP

(b) RPGM

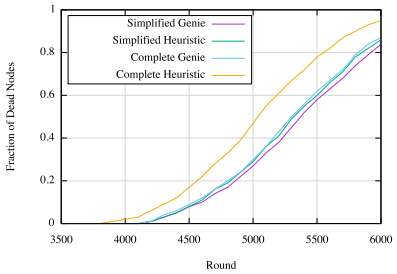

(c) MM

Figure 18: $F_{dn}(r, 50)$ for different values of r.

In Figure 19, we compare the mobility models, given that a certain charging policy is adopted. From Figures 19a, 19b and 19c we see that SGP, SHP and CGP behave in the same way, with the RPGM and MM curves being very tight and the RWP one being the worst one, in particular from round $r = 5000$ onward. Figure 19d, instead, shows that in CHP all the three mobility models are very tight and present the same performance.
Finally, Figure 20 compares all the results seen so far in this section.

To sum up, we see that, regardless of the mobility model in use, CGP and CHP provide, at the end of the simulation, a higher number of dead nodes than that of SGP and SHP. This fact, though, is not a fault in the designed complete policies, because they were not meant to optimise such parameter to begin with. Also, we can see that for all the policies we used, and for all the mobility models we adopted, approximately half of the nodes are still alive at round $r \approx 5000$, i.e., after 6.95h of simulation (we recall that the whole simulation lasts 8.33h), and we believe that most of the real-world users would have a chance to plug in their device before such time comes.

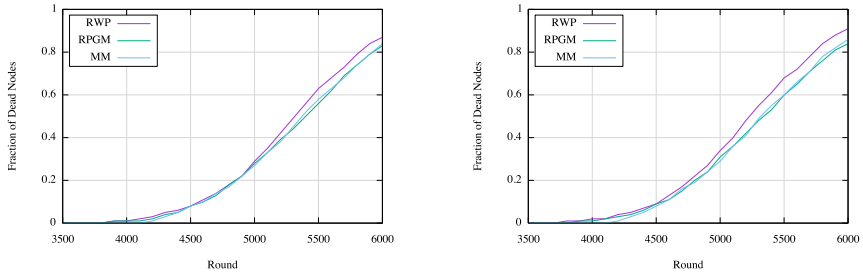

(a) Simplified Genie Policy

(b) Simplified Heuristic Policy

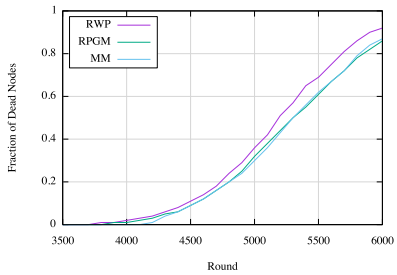

(c) Complete Genie Policy

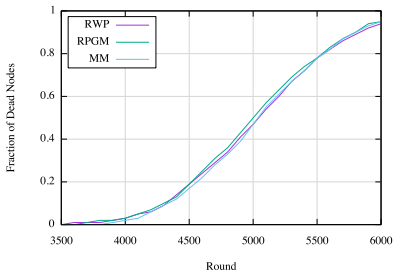

(d) Complete Heuristic Policy

Figure 19: $F_{dn}(r, 50)$ for different values of r. RWP , RPGM and MM are respectively shown in violet, light blue and green.

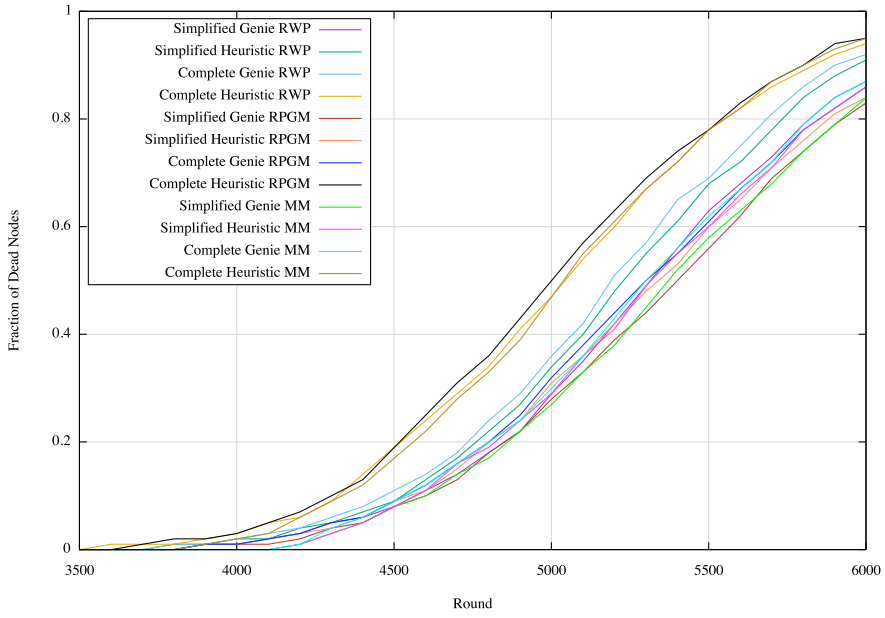

Figure 20: $F_{dn}(r, 50)$ for different values of r: comparison of all policies. RWP, RPGM and MM are shown.

4.1.4 *Average Battery Level per Round*

In this section, we briefly discuss the results regarding the average battery level of the nodes per round, $B_{avg}(r, N)$, reported in Equation 33, in the experiment with $N = 50$ nodes.

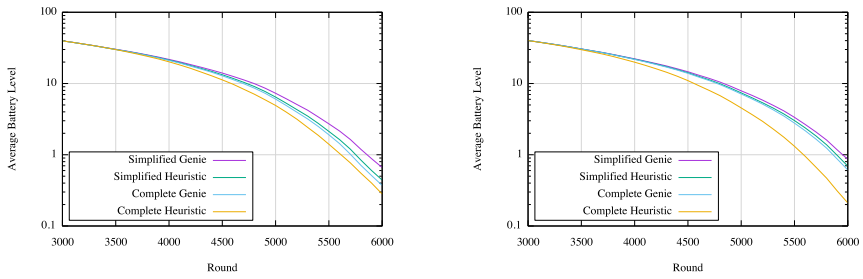

(a) RWP (b) RPGM

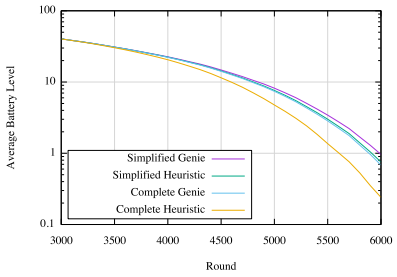

(c) MM

Figure 21: $B_{avg}(r, 50)$ for different values of r. Logarithmic scale is used for the y-axis.

Figure 21 shows the designed charging policies for each one of the mobility models we considered. As we expected, SGP is the one with the highest average battery level, followed by SHP, SGP and CHP for all the adopted mobility models.

Figure 22, instead, shows the average battery level of the three mobility models when a specific policy is fixed. The curves from all the models are very tight in both SGP and CHP of Figures 22a and 22d, while in SHP of Figure 22b and in CGP of Figure 22c RWP presents the one with the worst results.
As usual, in Figure 23 all the experiments are compared.

By comparing the general behaviour of the curves, we can see that, on average, the nodes start asking to be charged at round $r \approx 3500$, i.e., after 4.86h from the beginning of the simulation. From this round on, the base stations start receiving requests and, eventually, charging the nodes of the network, that survive, on average, other 2500 rounds, i.e., 3.47h, and, in some

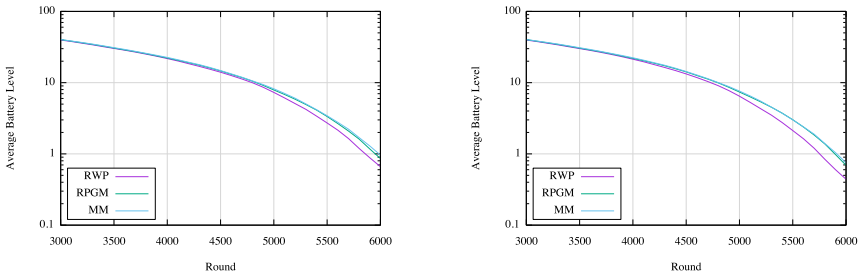

(a) Simplified Genie Policy

(b) Simplified Heuristic Policy

(c) Complete Genie Policy

(d) Complete Heuristic Policy

Figure 22: $B_{avg}(r, 50)$ for different values of r. RWP , RPGM and MM are respectively shown in violet, light blue and green. Logarithmic scale is used for the y-axis.

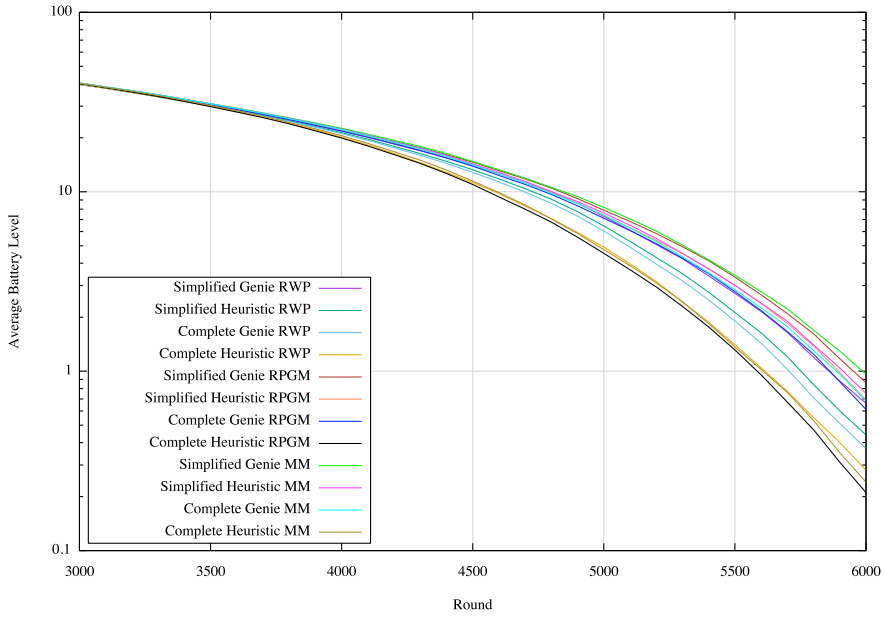

Figure 23: $B_{avg}(r, 50)$ for different values of r: comparison of all policies. RWP, RPGM and MM are shown. Logarithmic scale is used for the y-axis.

cases, are still alive after this period of time, when the simulation ends. This fact shows that, using the designed policies, the base stations permit the nodes to survive for a quite long extra period of time.

4.1.5 *Total Transmitted Energy*

In this section, we present the results regarding the total energy transmitted by the base stations throughout the simulation, $E_{TX}(tot)$, reported in Equation 28, i.e., the one related to the total transmitted power, for varying values of N. Figure 24 represents the case where RWP is used. We can see that SGP is the policy where the base stations consume more energy, followed by SHP and by CGP. In CHP, they consume much less, with $E_{TX}(tot) = 56J$ when $N = 10$ versus $E_{TX}(tot) \simeq 1.4kJ$ consumed by CGP for the same value of N. This trend continues as N grows.

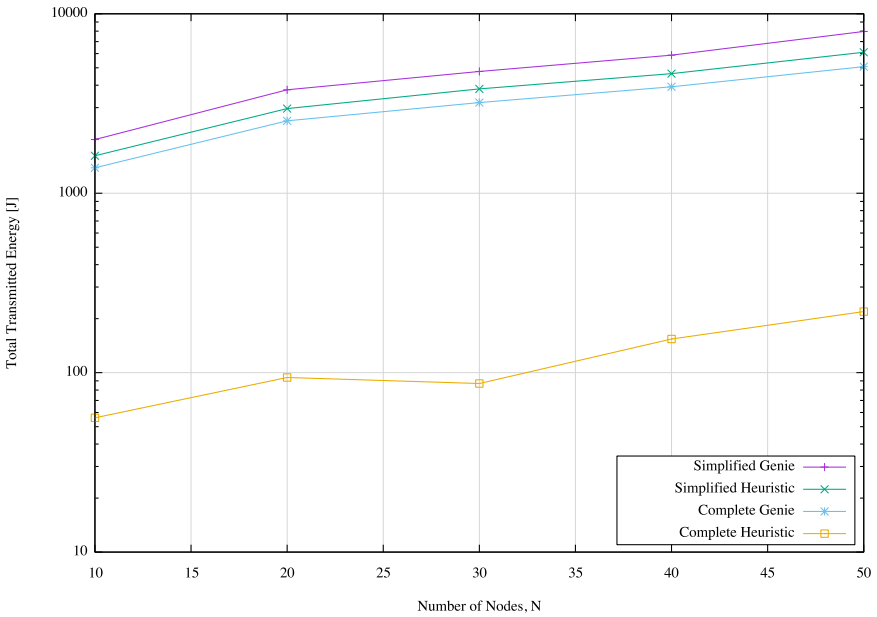

Figure 24: $E_{TX}(tot)$ for different values of N: RWP. Logarithmic scale is used for the y-axis.

The same considerations hold for both Figures 25 and 26, where the RPGM and MM cases are respectively shown.

Figure 27 shows the comparison between the transmitted energy when the various mobility models are applied and a specific charging policy is fixed. In SGP, and SHP of Figures 27a and 27b all the models behave in a similar way, with RWP and MM consuming almost the same amount of energy and RPGM

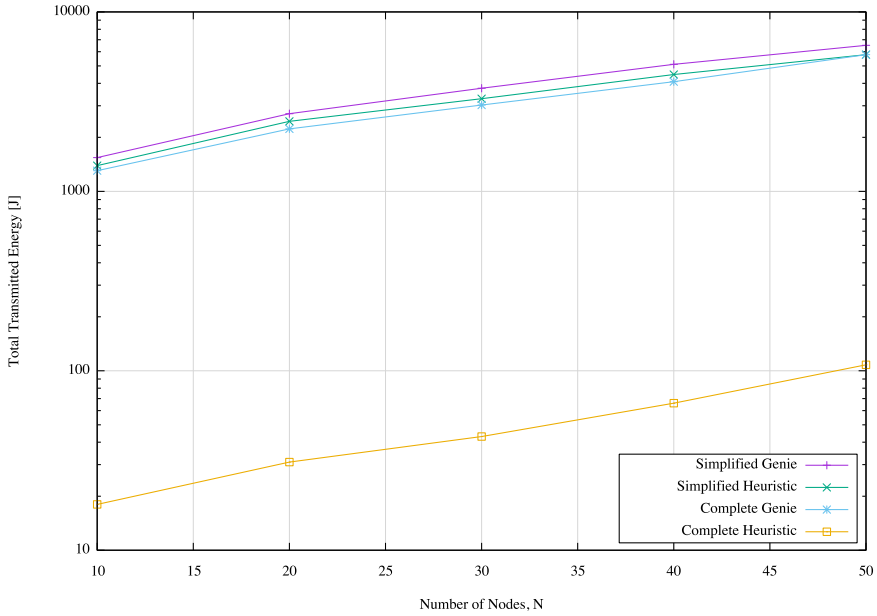

Figure 25: $E_{TX}(tot)$ for different values of N: RPGM. Logarithmic scale is used for the y-axis.

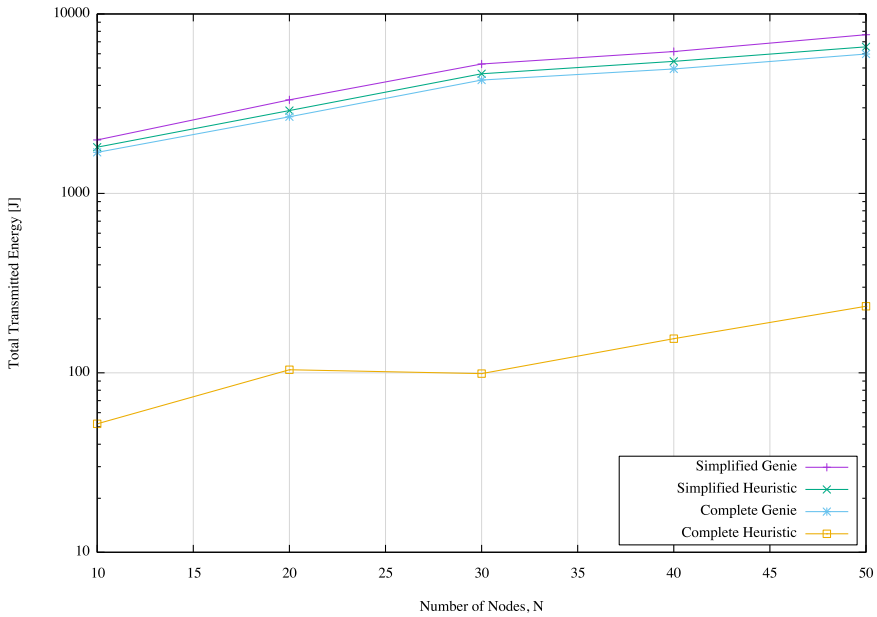

Figure 26: $E_{TX}(tot)$ for different values of N: MM. Logarithmic scale is used for the y-axis.

consuming slightly less. When N = 40, though, RWP reaches RPGM in the SHP case. In CGP of Figure 27c, instead, MM is the most energy-consuming model, while RWP and RPGM consume slightly less. Using CHP, shown in Figure 27d, the lowest amount of energy is consumed by the base stations throughout the simulation. In this case, RWP and MM present similar curves, while RPGM presents a much lower one. Using CHP, the base stations consume at least a tenth less energy than what they do employing the other policies. In all the considered policies, as expected, the amount of energy consumed by the base stations grows with an increasing N. This is due to the fact that a higher number of nodes join the network and, thus, a higher number of charging requests are made.

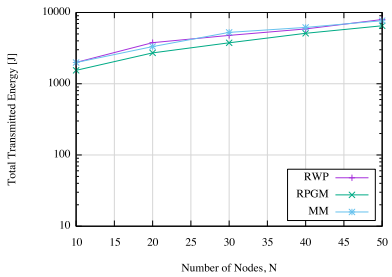

(a) Simplified Genie Policy

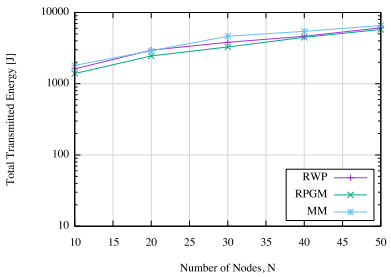

(b) Simplified Heuristic Policy

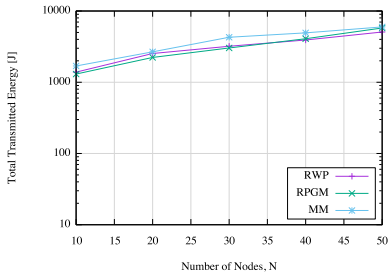

(c) Complete Genie Policy

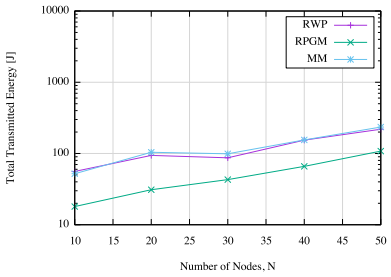

(d) Complete Heuristic Policy

Figure 27: $E_{TX}(tot)$ for different values of N. RWP , RPGM and MM are respectively shown in violet, light blue and green. Logarithmic scale is used for the y-axis.

Figure 28 shows the comparison of all the results seen in this section.

We saw that SGP and SHP are the most energy consuming policies, regardless of the adopted mobility model. As we previously observed from the results presented in Sections 4.1.2 and 4.1.3, though, they are also the ones reporting the lowest number of dead nodes. These two aspects confirm our previous conjecture that the simplified policies present a lower number

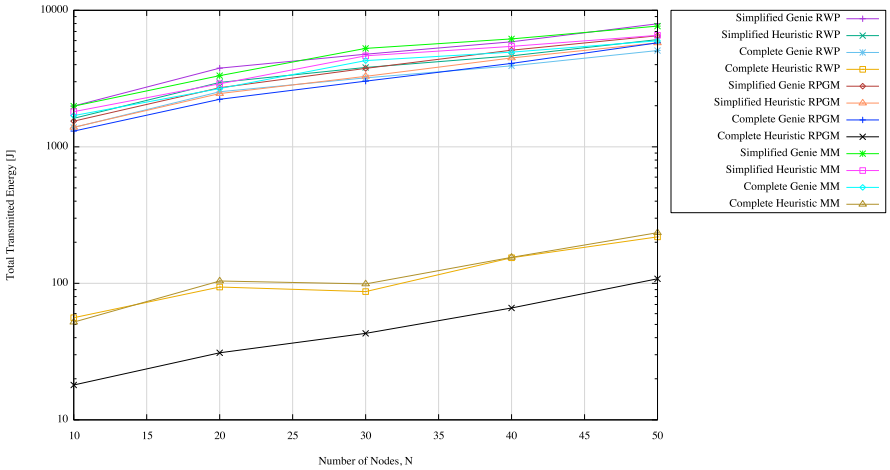

Figure 28: $E_{TX}(tot)$ for different values of N: comparison of all policies. RWP, RPGM and MM are shown. Logarithmic scale is used for the y-axis.

of dead nodes with respect to the complete ones because they transmit for a longer time, also due to the fact that, when they start doing so, they go on for a constant number Δ of rounds.

On the contrary, CGP and CHP are the ones with the highest number of dead nodes, but here we saw that the quantity of energy they consume is lower than the one consumed by the simplified policies, especially for high values of N, for instance when $N = 50$, where the difference between CHP in RPGM and SHP, or SGP, in RWP is respectively equal to 6kJ and 7.9kJ.

4.2 FAST MOBILITY SCENARIO

In this scenario, the maximum users' speed is $V_{max} = 42$ cells/round, that is equal to 30km/h, accounting for low-speed driving situations in densely deployed networks. The average user speed is equal to 15km/h. This case was studied to evaluate how the different speed of the users impacts on the proposed policies. In this section we highlight the main differences with the NM scenario, discussed in Section 4.1.

4.2.1 *Total Energy Efficiency*

In Figure 29, we compare the heuristic policies of the NM and FM models. As one can see, SHPs of the considered scenarios behave in the same way. In RWP, instead, the two scenarios perform in a similar way, while in RPGM FM is worse than NM.

In MM, instead, NM generally behaves better than FM, although, for short intervals, it performs slightly worse. From these results, we can say that this metric is not greatly affected by the users' speed.

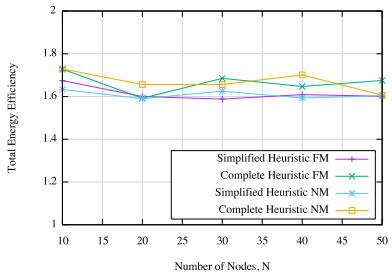

(a) RWP

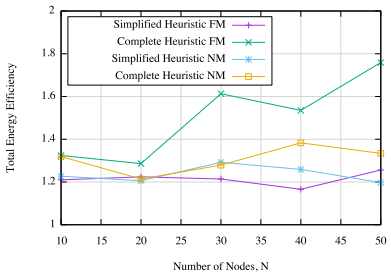

(b) RPGM

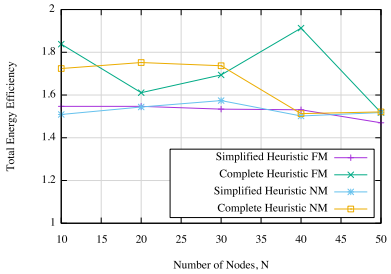

(c) MM

Figure 29: η_{tot} for different values of N. Comparison between heuristic policies of NM and FM.

The only noteworthy difference between the two models is shown in Figures 30, that reports the total energy efficiency when RPGM is used.

Comparing Figure 30 with RPGM in the NM case, we can see that SGP, SHP and CGP perform slightly better in FM, but CHP is quite worse, especially as N increases. This is probably due to the fact that is much more difficult to estimate nodes' positions in a high-speed scenario.
This tells us that, even in real-world driving scenarios, the designed policies behave well, especially for low values of N.

4.2.2 *Fraction of Dead Nodes*

Figure 31 compares the fraction of dead nodes for the heuristics in the NM and FM cases. Considering SHPs for the two different speeds, we see that they behave almost in the same way. Looking at CHPs, instead, we notice that the curve of the FM model

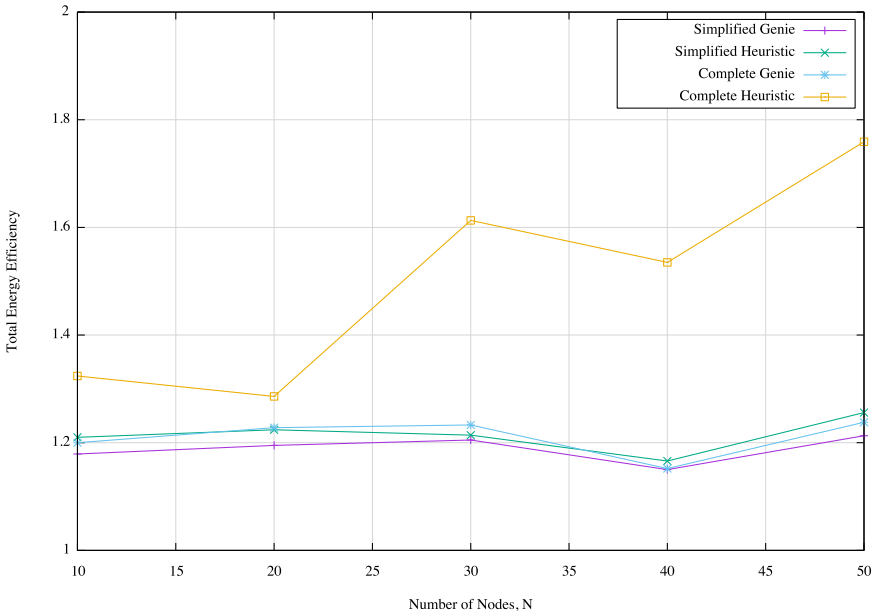

Figure 30: η_{tot} for different values of N in the FM scenario: RPGM.

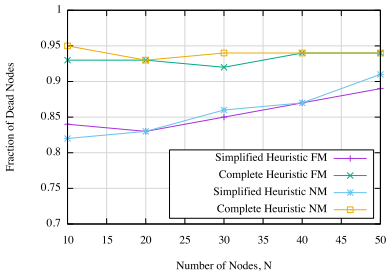

(a) RWP

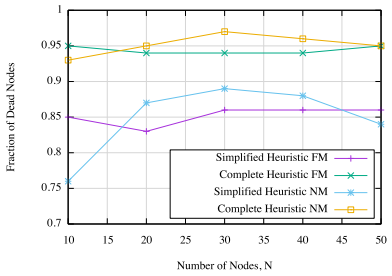

(b) RPGM

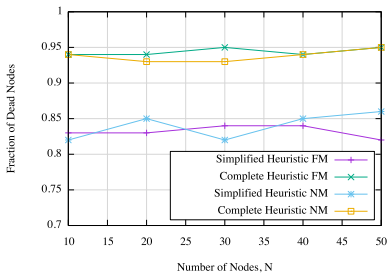

(c) MM

Figure 31: $F_{dn,tot}(N)$ for different values of N. Comparison between heuristic policies of NM and FM.

is generally below, or at the same level of the NM one, thus performing better, except in some cases, such as in MM when $N < 40$.

Two noteworthy differences with respect to the results presented for the NM scenario are shown in Figures 32 and 33. Figure 32 represents RPGM when the FM scenario is considered. Comparing this plot to the NM one, shown in Figure 14, we can see that all the curves, but CHP assume lower values when $N = 10$, while they reach similar ones for $N = 50$. Also, in this case, they do not present the concave behaviour we noticed in the NM case, but tend to stabilise on a certain value and, then, keep it from $N = 30$ onward.

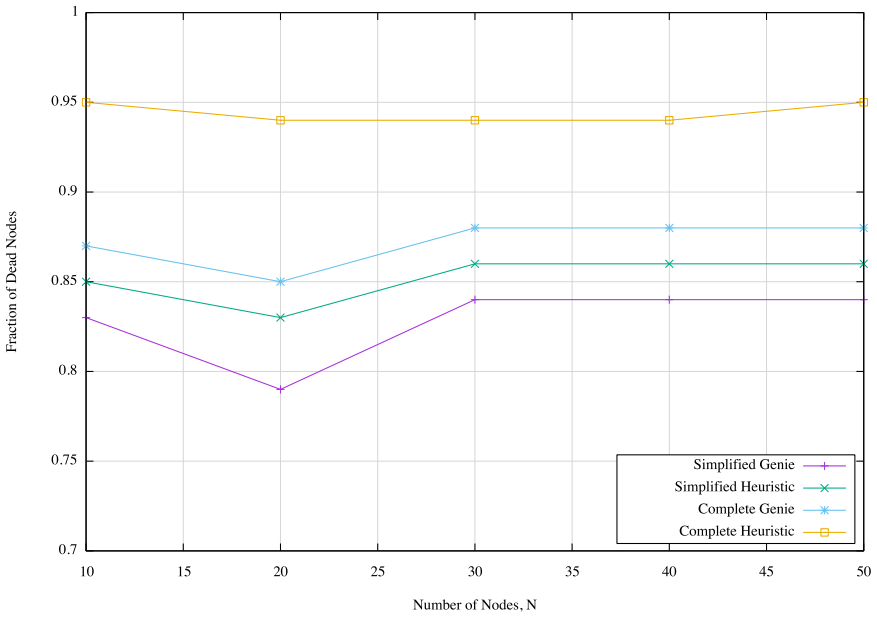

Figure 32: $F_{dn,tot}(N)$ for different values of N in the FM scenario: RPGM.

Figure 33, instead, shows MM when the FM scenario is considered. Comparing these results with the NM ones, shown in Figure 15, we can see that the curves related to SGP, SHP and CGP, although, in general, assuming higher values for $N = 10$, are more stable than the NM ones as N grows, and reach quite smaller values for $N = 50$.

These results indicate that, even in a driving scenario, the number of dead nodes is not worsened with respect to a pedestrian one and, in some cases, it is even better than that of the walking case.

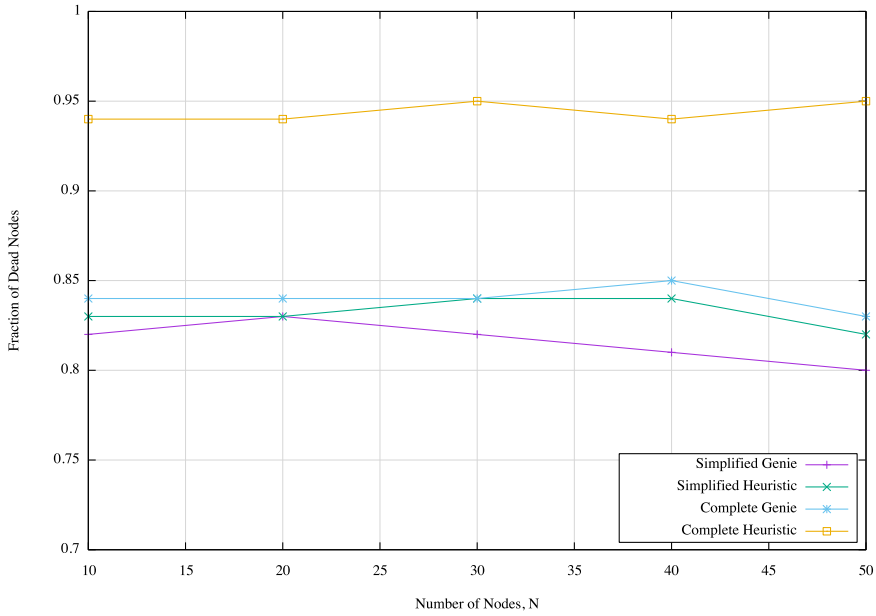

Figure 33: $F_{dn,tot}(N)$ for different values of N in the FM scenario: MM.

4.2.3 *Dead Nodes and Average Battery Level per Round*

Figures 34 and 35 respectively show $F_{dn}(r, 50)$ and $B_{avg}(r, 50)$ for different values of r in the FM scenario.
As we can see, these results are similar to those reported in Figures 18 and 21 and, thus, analogous considerations hold.

4.2.4 *Total Transmitted Energy*

Figure 36 reports the total transmitted energy $E_{TX}(tot)$ when the heuristic policies are applied in the NM and FM scenarios for the three considered mobility models. As we can see, SHPs of both the NM and FM cases are quite similar, with, in general, the former consuming slightly less energy than the latter.

Regarding CHPs, instead, the base stations of FM consume considerably less energy than those of NM. This is due to the fact that, when NM is used, the nodes spend a higher number of rounds inside the charging area of the base stations, compared to that they spend in FM, because of the reduced users' speed, and, thus, a higher number of rounds than that of FM is involved in the charging process, making the base stations use a higher amount of energy than that they spend with FM. The only case in which NM and FM consume a similar amount of energy is when RWP is adopted and $N = 30$, where FM consumes

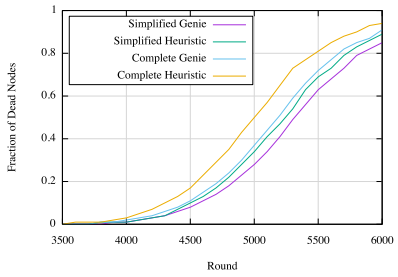

(a) RWP

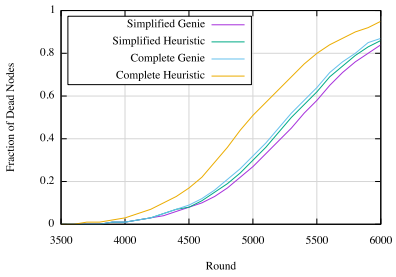

(b) RPGM

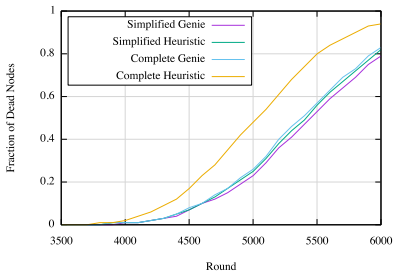

(c) MM

Figure 34: $F_{dn}(r, 50)$ for different values of r in the FM scenario.

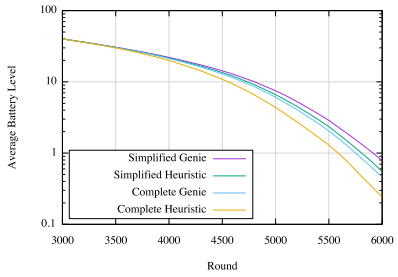

(a) RWP

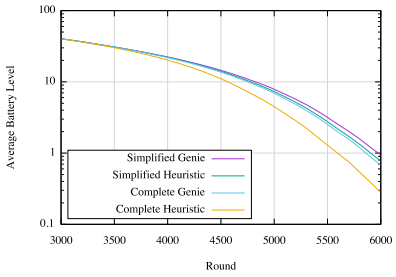

(b) RPGM

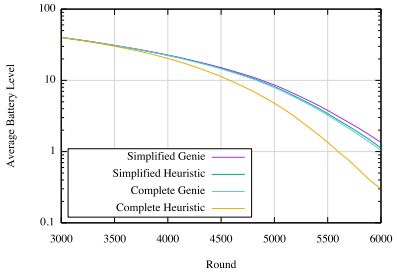

(c) MM

Figure 35: $B_{avg}(r, 50)$ for different values of r in the FM scenario. Logarithmic scale is used for the y-axis.

slightly more energy than NM and then, for $N > 30$, it returns consuming a lower amount energy than NM.

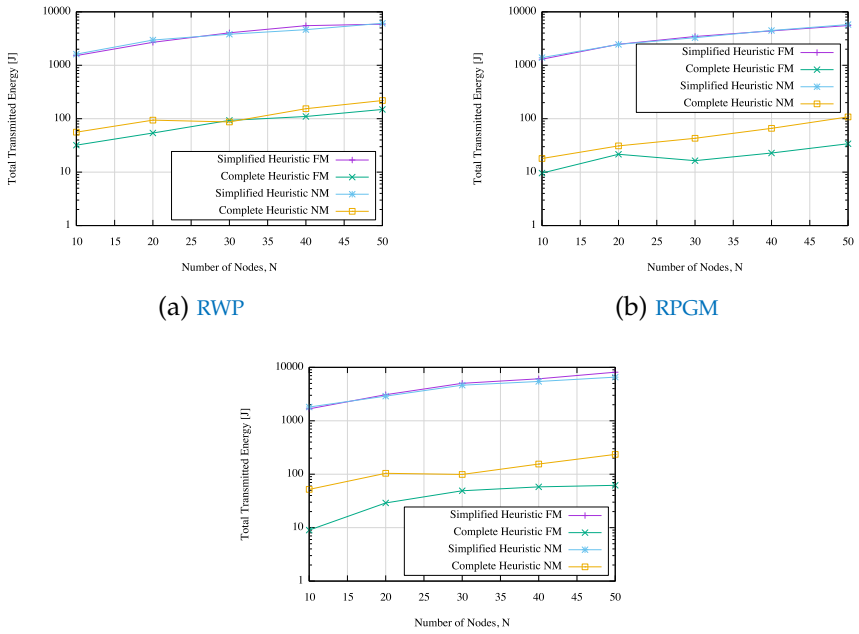

(a) RWP (b) RPGM

(c) MM

Figure 36: $E_{TX}(tot)$ for different values of N. Comparison between heuristic policies of NM and FM.

After examining the results discussed so far, we can conclude that mobility speed does not greatly affect the designed charging policies regarding the energy efficiency, the dead nodes or their battery curves. Instead, it influences the total energy consumed by the base stations of the network when CHP is used.

To conclude this chapter, we underline that a tradeoff between energy efficiency, transmitted energy and fraction of dead nodes is necessary: it is not possible to optimise all these metrics, at least not with the kind of policies we designed, and which one to use depends on the particular applications at hand.

5

CONCLUSIONS AND FUTURE WORKS

In this work we studied the Wireless Power Transfer technique for Next Generation Mobile Networks. Specifically, the considered scenario involved fixed base stations placed around the network and a variable number of users travelling through it and requiring the base stations to be charged, if necessary.

We implemented three different mobility models to simulate UEs moving along the network: the Random Waypoint Model, that considers random users moving independently from one another, the Reference Point Group Mobility Model, that permits to study the movement of a group of users, or, alternatively, that of a single user carrying multiple devices with him, and the Manhattan Mobility Model, that considers UEs moving in geographically restricted areas, such as urban environments.

We designed two policies, the simplified heuristic policy and the complete heuristic one, basing on which the base stations of the network decide whether to charge the battery of energy-requiring devices, or not. In both our policies, the base stations examine a window of W rounds and observe the devices currently inside their coverage area, i.e., those they could wirelessly charge. In SHP a base station starts transferring power in the round in which the greatest number of users is inside its coverage area, and then continues the transfer for a fixed number of rounds Δ. In CHP, instead, it also estimates the future arrivals and departures of the nodes from its coverage area and computes the transfer efficiency $\eta(r_s, r_e)$ for all the pairs of rounds (r_s, r_e) inside the looking window $\mathcal{W}$. Then the base station selects as starting and ending rounds of the wireless transfer process the pair of rounds presenting the lowest efficiency value, in order to minimise this metric.

To analyse the behaviour of the designed policies, we compared each one of them with the corresponding genie policy, that, due to the fact that it knows everything about the network and its devices, indicates how the performance of the related heuristic should go. Moreover, we also briefly discussed the computational complexity of the heuristic policies, forecasting a possible real-world implementation of these.

In order to evaluate the performance of the proposed policies, we wrote a network simulator in C language and ran a large number of experiments, simulating more than 8 hours of the real-world time. The measured metrics were the total energy efficiency, the fraction of dead nodes at the end of the simulation, the dead nodes and the average battery level per round and the total transmitted energy. We also compared the normal-speed mobility pedestrian scenario with a fast-speed driving one, to see how different users' speeds affect the system performance.

Considering the total transfer efficiency, we saw that, even with the simplified policies, it reaches values comparable with those of the complete ones, especially as the number of nodes, N, grows. The simplified policies also present a lower number of dead nodes at the end of the simulation, due to the fact that, when adopting them, the base stations transmit, on average, more energy, as demonstrated by the results regarding the total transmitted energy. It is interesting to note that, in CHP, the number of dead nodes, in general, decreases as N increases, due to the fact that, even if it is difficult for this policy to forecast the future position of UEs and wrong estimates are possible, when many nodes are in the network, a fraction of them will be inside the coverage area of the base station anyway.

Looking at the dead nodes per round of the simulation, we saw that, regardless of the mobility model in use, the complete policies present a higher number of UEs whose battery completely exhausted during the simulation. This is not a fault of the designed policies, though, because they were not designed to optimise such metric, but only to minimise the transfer efficiency, objective that they reach in a pretty good way. Moreover, we can see that for all the policies we used, and for all the implemented mobility models, approximately half of the nodes survive almost until the end of the simulation, i.e., until 6.95 hours have passed, and we believe that most of the real-world users would have a chance to plug in their device before such time comes. The average battery level per round follows the same behaviour and, thus, the same considerations hold.

From the total transmitted energy, instead, we saw that when using the complete policies, even if reporting a higher fraction of dead nodes with respect to the simplified ones, the base stations end up transmitting a tremendously lower amount of energy than what done with the simplified policies, especially when CHP is used, thus presenting a lower cost in the real world, although reaching equally good performance.

Comparing the normal-speed pedestrian scenario with the fast-speed driving one, we can safely tell that a different speed of the users does not largely affect the energy efficiency, the dead nodes or their battery curves. Instead, it influences the total energy consumed by the base stations of the network, in particular, when CHP is employed.

All the mobility models we studied presented similar behaviours, with RPGM being slightly better than the other two, due to the fact that multiple devices move following the same path, thus affecting the number of simultaneously chargeable devices in a greater way.

Finally, we think that a tradeoff between energy efficiency, transmitted energy and fraction of dead nodes is necessary: it is not possible to optimise all these metrics and which policy to use depends on the particular applications at hand.

Given that the performance of the whole designed system is greatly influenced by the transfer efficiency function $\mu_n(d)$, reported in Equation 23, in a future work it would be interesting to find another function to model the transfer efficiency, that permits to reach further distances than what possible with the one used here.

One could also design appropriate business models to include a fee payed by the nodes in exchange for the received energy, possibly also including different prices depending on the number of energy-requiring users inside a base station's coverage area. Such function, in fact, could be inversely proportional to the number of UEs that a base station can simultaneously charge.

Another possible future development is a model in which the network's base stations harvest the energy they will, then, provide to the nodes from both environmental sources, e.g., solar panels.

Furthermore, it would be interesting to design policies that try to jointly optimise the total energy efficiency, total transmitted energy and fraction of dead nodes. Beamforming is also to be studied for power transmission at the base stations.

BIBLIOGRAPHY

[1] Sunila Akbar, Yansha Deng, Arumugam Nallanathan, Maged Elkashlan, and Abdol-Hamid Aghvami. «Simultaneous Wireless Information and Power Transfer in K -Tier Heterogeneous Cellular Networks». In: *IEEE Transactions on Wireless Communications* 15.8 (Aug. 2016), pp. 5804–5818.

[2] Dogay Altinel and Gunes Karabulut Kurt. «Energy Harvesting from Multiple RF Sources in Wireless Fading Channels». In: *IEEE Transactions on Vehicular Technology* PP.99 (Jan. 2016), pp. 1–11.

[3] Pham T. Anh and Ming-Hung Chen. «Design and optimization of high-efficiency resonant wireless power transfer system». In: *International Conference on System Science and Engineering*. Nantou County, TW, July 2016.

[4] Fan Bai and Ahmed Helmy. «A survey of mobility models». In: *Wireless Adhoc Networks* 206 (June 2004), pp. 147–176.

[5] Fan Bai, Narayanan Sadagopan, and Ahmed Helmy. «IMPORTANT: a framework to systematically analyze the Impact of Mobility on Performance of Routing Protocols for Adhoc Networks». In: *Annual Joint Conference of the IEEE Computer and Communications*. San Francisco, CA, US, Mar. 2003.

[6] Javier Blanco, Ferran Bolos, Ana Collado, and Apostolos Georgiadis. «RF-energy harvesting and wireless power transfer efficiency from digitally modulated signals». In: *IEEE Mediterranean Microwave Symposium*. Lecce, IT, Nov. 2015.

[7] Josh Broch, David A. Maltz, David B. Johnson, Yih-Chun Hu, and Jorjeta Jetcheva. «A performance comparison of multi-hop wireless ad hoc network routing protocols». In: *ACM/IEEE international conference on Mobile computing and networking*. Dallas, TX, US, Oct. 1998.

[8] Jean-Marc Collignon, Alexis Quement, Bruno B. Picdi, Badr Rmili, and Amaya Espinosa. «RFID and RF harvesting wireless sensor network platform for launcher applica-

tion». In: *IEEE International Conference on Wireless for Space and Extreme Environments*. Orlando, FL, US, Dec. 2015.

[9] Yansha Deng, Lifeng Wang, Maged Elkashlan, Marco Di Renzo, and Jinhong Yuan. «K-tier heterogeneous cellular networks with wireless power transfer». In: *IEEE International Conference on Communications*. Kuala Lumpur, MY, May 2016.

[10] Yansha Deng, Lifeng Wang, Maged Elkashlan, Marco Di Renzo, and Jinhong Yuan. «Modeling and Analysis of Wireless Power Transfer in Heterogeneous Cellular Networks». In: *IEEE Transactions on Communications* PP.99 (June 2016), pp. 1–14.

[11] Marco Di Renzo and Wei Lu. «System-Level Analysis/Optimization of Cellular Networks with Simultaneous Wireless Information and Power Transfer: Stochastic Geometry Modeling». In: *IEEE Transactions on Vehicular Technology* PP.99 (May 2016), pp. 1–24.

[12] Francesco Guidolin, Irene Pappalardo, Andrea Zanella, and Michele Zorzi. «Context-Aware Handover Policies in HetNets». In: *IEEE Transactions on Wireless Communications* 15.3 (Mar. 2016), pp. 1895–1906.

[13] Liang He, Peng Cheng, Yu Gu, Jianping Pan, Ting Zhu, and Cong Liu. «Mobile-to-mobile energy replenishment in mission-critical robotic sensor networks». In: *IEEE Conference on Computer Communications*. Toronto, ON, CA, Apr. 2014.

[14] Tengjiao He, Kwan-Wu Chin, and Sieteng Soh. «On Wireless Power Transfer and Max Flow in Rechargeable Wireless Sensor Networks». In: *IEEE Access* 4 (Aug. 2016), pp. 4155–4167.

[15] *Internet Live Stats*. Sept. 2016. URL: http://www.internetlivestats.com/.

[16] Jouya Jadidian and Dina Katabi. «Magnetic MIMO: How to Charge Your Phone in Your Pocket». In: *Annual International Conference on Mobile Computing and Networking*. Maui, HI, US, Sept. 2014.

[17] David B. Johnson and David A. Maltz. «Dynamic Source Routing in Ad Hoc Wireless Networks». In: *Mobile Computing*. Ed. by Tomasz Imielinski and Henry F. Korth. Boston, MA, US: Springer US, 1996, pp. 153–181.

[18] Lyes Khelladi, Djamel Djenouri, Michele Rossi, and Nadjib Badache. «Efficient On-Demand Multi-Node Charging Techniques for Wireless Sensor Networks». Submitted. 2016.

[19] André Kurs, Aristeidis Karalis, Robert Moffatt, John D. Joannopoulos, Peter Fisher, and Marin Soljačić. «Wireless Power Transfer via Strongly Coupled Magnetic Resonances». In: *Science* 317.5834 (July 2007), pp. 83–86.

[20] André Kurs, Robert Moffatt, and Marin Soljačić. «Simultaneous mid-range power transfer to multiple devices». In: *Applied Physics Letters* 96.4 (Jan. 2010), 044102:1–044102:3.

[21] Chi Lin, Guowei Wu, Mohammad S. Obaidat, and Chang Wu Yu. «Clustering and splitting charging algorithms for large scaled wireless rechargeable sensor networks». In: *Journal of Systems and Software* 113 (Mar. 2016), pp. 381–394.

[22] Chong-Li Liou, Chi-Jung Kuo, and Shau-Gang Mao. «Wireless-Power-Transfer System Using Near-Field Capacitively Coupled Resonators». In: *IEEE Transactions on Circuits and Systems II: Express Briefs* 63.9 (Sept. 2016), pp. 898–902.

[23] Sudha Lohani, Roya A. Loodaricheh, Ekram Hossain, and Vijay K. Bhargava. «On Multiuser Resource Allocation in Relay-Based Wireless-Powered Uplink Cellular Networks». In: *IEEE Transactions on Wireless Communications* 15.3 (Mar. 2016), pp. 1851–1865.

[24] Xiao Lu, Dusit Niyato, Ping Wang, Dong In Kim, and Zhu Han. «Wireless charger networking for mobile devices: fundamentals, standards, and applications». In: *IEEE Wireless Communications* 22.2 (Apr. 2015), pp. 126–135.

[25] Xiao Lu, Ping Wang, Dusit Niyato, and Zhu Han. «Resource allocation in wireless networks with RF energy harvesting and transfer». In: *IEEE Network* 29.6 (Nov. 2015), pp. 68–75.

[26] Xiao Lu, Ping Wang, Dusit Niyato, and Ekram Hossain. «Dynamic spectrum access in cognitive radio networks with RF energy harvesting». In: *IEEE Wireless Communications* 21.3 (June 2014), pp. 102–110.

[27] Deepak Mishra, Swades De, and Kaushik R. Chowdhury. «Charging Time Characterization for Wireless RF Energy Transfer». In: *IEEE Transactions on Circuits and Systems II: Express Briefs* 62.4 (Apr. 2015), pp. 362–366.

[28] Ali A. Nasir, Xiangyun Zhou, Salman Durrani, and Rodney A. Kennedy. «Relaying Protocols for Wireless Energy Harvesting and Information Processing». In: *IEEE Transactions on Wireless Communications* 12.7 (June 2013), pp. 3622–3636.

[29] Dusit Niyato and Ping Wang. «Competitive wireless energy transfer bidding: A game theoretic approach». In: *IEEE International Conference on Communications*. Sydney, NSW, AU, June 2014.

[30] Wasiu O. Popoola and Evangelos Pikasis. «On visible light communication and quality of light emitted from illumination LEDs». In: *IEEE Photonics Society Summer Topical Meeting Series*. Newport Beach, CA, USA, July 2016.

[31] *Powercast*. Aug. 2016. URL: http://www.powercastco.com/.

[32] *Qi*. Wireless Power Consortium. July 2016. URL: https://www.wirelesspowerconsortium.com/.

[33] Sean Rocke. «Out-of-band radiation: Opportunities for antenna-based RF energy harvesting in wireless devices?» In: *IEEE Online Conference on Green Communications*. Piscataway, NJ, US, Nov. 2015.

[34] Ryan Sasur. *Wireless Energy Transfer*. 2011.

[35] Min Sheng, Liang Wang, Xijun Wang, Yan Zhang, Chao Xu, and Jiandong Li. «Energy Efficient Beamforming in MISO Heterogeneous Cellular Networks With Wireless Information and Power Transfer». In: *IEEE Journal on Selected Areas in Communications* 34.4 (Apr. 2016), pp. 954–968.

[36] Ruijin Sun, Ying Wang, Zhongyu Miao, and Xinshui Wang. «Destination-aided Wireless Power Transfer in Energy-limited Cognitive Relay Systems». In: *IEEE Access* PP.99 (Aug. 2016), pp. 1–12.

[37] Shaista Tarannum. «Data Transmission Through Smart Illumination via "Visible Light Communication Technology"». In: *International Journal of Technical Research and Applications* 4.2 (Apr. 2016), pp. 136–141.

[38] Tu Lam Thanh, Marco Di Renzo, and Justin P. Coon. «MIMO cellular networks with Simultaneous Wireless Information and Power Transfer». In: *IEEE International Workshop on Signal Processing Advances in Wireless Communications*. Edinburgh, UK, July 2016.

[39] Lav R. Varshney. «Transporting information and energy simultaneously». In: *IEEE International Symposium on Information Theory*. Toronto, ON, CA, July 2008.

[40] Hubregt J. Visser and Ruud J. M. Vullers. «RF Energy Harvesting and Transport for Wireless Sensor Network Applications: Principles and Requirements». In: *Proceedings of the IEEE* 101.6 (June 2013), pp. 1410–1423.

[41] Liguang Xie, Yi Shi, Y. Thomas Hou, and Hanif D. Sherali. «Making sensor networks immortal: An energy-renewal approach with wireless power transfer». In: *IEEE/ACM Transactions on Networking* 20.6 (Feb. 2012), pp. 1748–1761.

[42] Jing Yang and Sennur Ulukus. «Optimal Packet Scheduling in an Energy Harvesting Communication System». In: *IEEE Transactions on Communications* 60.1 (Jan. 2012), pp. 220–230.

[43] Zizhen Zeng, Xing Li, Amine Bermak, Chi-Ying Tsui, and Wing-Hung Ki. «A WLAN 2.4-GHz RF energy harvesting system with reconfigurable rectifier for wireless sensor network». In: *IEEE International Symposium on Circuits and Systems*. Montreal, QC, CA, May 2016.

[44] Rui Zhang and Chin K. Ho. «MIMO Broadcasting for Simultaneous Wireless Information and Power Transfer». In: *IEEE Global Telecommunications Conference*. Houston, TX, US, Dec. 2011.

A

ACRONYMS

AC	Alternating Current
CGP	Complete Genie Policy
CHP	Complete Heuristic Policy
DC	Direct Current
EIRP	Effective Isotropic Radiated Power
FM	Fast Mobility
HCN	Heterogeneous Cellular Network
HetNet	Heterogeneous Network
IoT	Internet of Things
ISM	Industrial, Scientific and Medical
LoS	Line of Sight
MC	Mobile Charger
MIMO	Multiple Input Multiple Output
MISO	Multiple Input Single Output
MM	Manhattan Model
NM	Normal Mobility
QoS	Quality of Service
RF	Radio Frequency
RFID	Radio Frequency Identification
RPGM	Reference Point Group Mobility Model
RSSI	Received Signal Strength Indicator
RWP	Random Waypoint Model
SGP	Simplified Genie Policy

SHP	Simplified Heuristic Policy
SI	Système International d'Unités (French for International System of Units)
SNR	Signal-to-Noise-Ratio
SWIPT	Simultaneous Wireless Information and Power Transfer
UE	User Equipment
UHF	Ultra High Frequency
WCV	Wireless Charging Vehicle
WLAN	Wireless Local Area Network
WPT	Wireless Power Transfer
WSN	Wireless Sensor Network

B

NOTATION

Symbol	Meaning
A_{bs}	base station's coverage area
B	number of base stations in the network
$B_{avg}(r, N)$	average battery level of the nodes per round
bs	generic base station
$\mathbf{bs} = [bs_0, \ldots, bs_{B-1}]$	base stations' vector
d	distance between node and base station [m]
E	energy [J]
E_{RX}	energy received at the node [J]
E_{TX}	energy related to the power transmitted by the base station [J]
E_{max}	maximum node's battery energy [J]
$E_{q,max}$	maximum energy discharge quantity per round [J]
E_{safe}	threshold for a node to deleting a charging request [%]
E_{thr}	threshold for a node to issue a charging request [%]
$e(n)$	indicator function of whether the node needs to be charged or not
$F_{dn}(r, N)$	fraction of dead nodes at round r
$F_{dn,tot}$	fraction of dead nodes at the end of the simulation
f	frequency
G_{el}	number of nodes belonging to the same group
G_{RX}	receive antenna gain

To be continued in the next page

Continued from the previous page

Symbol	Meaning
G_{TX}	transmit antenna gain
$i(n)$	indicator function of whether the node is inside A_{bs} or not
L_b	length of the edge of a block [cells]
M_i, $i \in \{1, 2\}$	dimension of the network matrix [cells]
N	number of nodes in the network
N_{dn}	number of dead nodes
N_{ins}	number of nodes inside A_{bs}
n	generic node
$\mathbf{n} = [n_0, \ldots, n_{N-1}]$	nodes' vector
P_L	path loss
$P_{RX}(d)$	power received at the node [W]
P_{TX}	power transmitted by the base station [W]
$\mathbf{p} = [p_x, p_y]$	position of the node in the network
p_{disch}	battery discharge probability
R	number of rounds of the simulation
R_{ch}	charging radius of the base station [m]
$R_{ch,max}$	maximum value for R_{ch} [m]
R_{cnt}	control granularity [rounds]
r	generic round
r^*	optimal round
r_e	round in which to end the charging process
r_s	round in which to start the charging process
ΔT	duration of a single round [s]
T_{pause}	pause time of a node after reaching its destination [rounds]
V_{max}	maximum speed of a node [cells/round]

To be continued in the next page

Continued from the previous page

Symbol	Meaning
$\boldsymbol{v} = [v_x, v_y]$	speed of a node [cells/round]
$\mathcal{W}$	looking window
W	number of rounds of the looking window
Δ	number of consecutive charging rounds of the simplified policies
$\eta(r_s, r_e)$	energy efficiency function computed from round r_s to round r_e
η_{tot}	total energy efficiency function of the whole simulation
λ	wavelength
$\mu(d)$	transfer efficiency function of wireless power transfer

Concluded from the previous page